Nanomaterials

DOI: 10.1002/anie.201310803

Diamond Nanowires: Fabrication, Structure, Properties, and Applications

*Yuan Yu, Liangzhuan Wu, and Jinfang Zhi**

Keywords:
diamond · nanomaterials · nanopillars · nanorods · nanowires

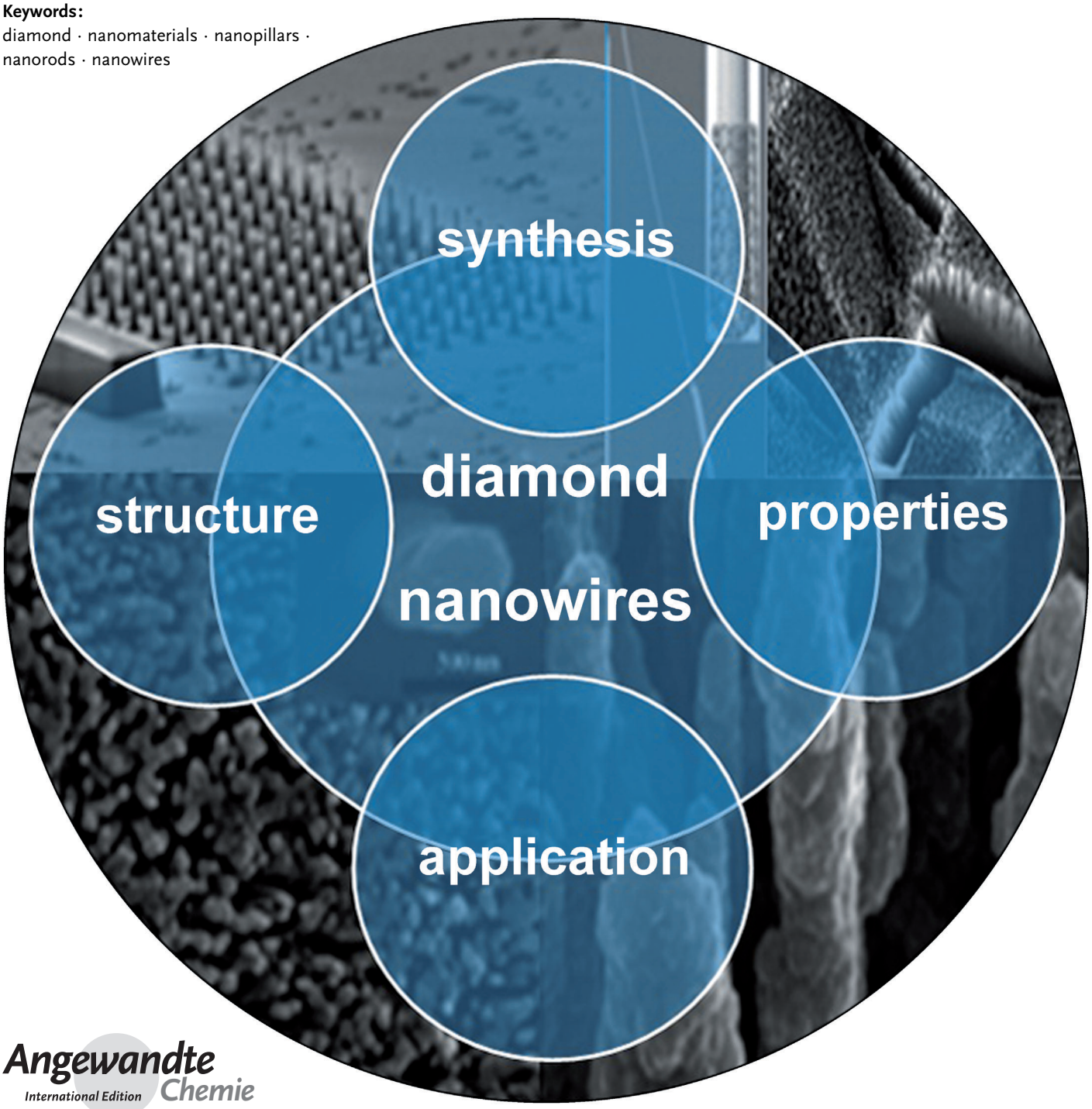

C(sp^3)–C-bonded diamond nanowires are wide band gap semiconductors that exhibit a combination of superior properties such as negative electron affinity, chemical inertness, high Young's modulus, the highest hardness, and room-temperature thermal conductivity. The creation of 1D diamond nanowires with their giant surface-to-volume ratio enhancements makes it possible to control and enhance the fundamental properties of diamond. Although theoretical comparisons with carbon nanotubes have shown that diamond nanowires are energetically and mechanically viable structures, reproducibly synthesizing the crystalline diamond nanowires has remained challenging. We present a comprehensive, up-to-date review of diamond nanowires, including a discussion of their synthesis along with their structures, properties, and applications.

From the Contents

1. Introduction

Diamond is a material of extremes. As a result of its unique combination of properties, such as wide band gap, negative electron affinity, chemical inertness, resistance to particle bombardment, extreme hardness, and thermal conductivity, diamond is a promising material for applications in various fields.[1–3] These properties of crystalline diamond originate from the diamond lattice structure and the strong carbon–carbon bond. Doping process can improve the electrical properties of diamond. Heavily boron-doped diamond (BDD) has been recognized as one of the most promising electrode materials for electrochemical applications[4,5] because of its unique features such as high chemical stability, wide potential window, negligible capacitive current, and high biocompatibility. Metal catalysts are expected to be stable on diamond because of the formation of metal carbides. Defects also play an important role, often a beneficial one, on the properties of diamond. Color centers are an example of such benefits.[6] Light-emitting defects (color centers) in diamond are increasingly attractive for their implementation in a solid-state platform. For example, color centers based on nitrogen,[7–9] silicon,[10] carbon,[11] nickel,[12] and chromium[13] impurities have been shown to generate nonclassical states of light and emit single photons at room temperature, which is a critical resource for quantum optical communication systems. Of these defects, the nitrogen-vacancy (NV) center is very attractive, since it can possess additional electron and nuclear spin degrees of freedom with long coherence times that act as a quantum memory for long-distance quantum communications.[14,15] In addition, because the dislocation movement is hindered by the impurities, the toughness and wear resistance of diamond may increase as its impurity content increases.

As a consequence of these unique features and the high value of natural diamond, tremendous attention has been paid to manufacturing diamonds and diamond-like carbon (DLC) since the first artificial diamond was synthesized in the 1950s. The techniques, which range from the direct solid-state transformation of graphite under static or shock pressure to chemical-vapor deposition, allow the synthesis of materials with properties approaching those of natural diamond. Recently, the synthesis and characterization of nanometer-sized clusters, including nanocrystalline films of diamond-like carbon and nano- and polycrystalline cubic diamond, has attracted special attention.[16–18] These studies are motivated by the observed ability to vary the properties of these materials through their size.[19] Ultrafine diamond synthesized by explosive detonation was proposed to be very interesting for many traditional diamond applications, such as the fine polishing of ceramics and surface coatings. Polycrystalline cubic diamond obtained by the direct conversion of graphite at static high pressures and temperatures is extremely hard.[20] However, it was synthesized in microscopic quantities, but that was not sufficient for full characterization of the physical properties of the sample. The first synthesis of a bulk sample of nanocrystalline diamond from C_{60} was recently reported,[21] and intensive investigation has suggested that the new material was at least as hard as single-crystal diamond and, at high temperature and ambient pressure, kinetically more stable with respect to graphitization than usual diamonds.

Nanowires fabricated using top-down and/or bottom-up procedures have characteristics of low weight with sometimes extraordinary mechanical, electrical, thermal, and multifunctional properties.[22,23] Nanowires can be used for the tunable transport of electrons, with the electronic properties strongly influenced by small perturbations of the surface, which allows large surface-to-volume ratio enhancements. Theoretical evaluations of the properties of diamond nanowires and nanorods,[24–27] which predicted superior properties of diamond nanowires and made them an important and viable target for synthesis, encouraged our search for methods for their production. As a result of the numerous efforts, many methods for the synthesis of diamond nanowires have been developed, including reactive-ion etching (RIE),[28–35] plasma post-treatment of carbon nanotubes,[36,37] transfer of ful-

[*] Dr. Y. Yu, Dr. L. Wu, Prof. Dr. J. Zhi
Key Laboratory of Photochemical Conversion and Optoelectronic Materials, Technical Institute of Physics and Chemistry, Chinese Academy of Sciences, Beijing, 100190 (P.R. China)
E-mail: zhi-mail@mail.ipc.ac.cn

lerenes to diamond nanowires at high temperatures and high pressures,[38] and template- or catalyst-assisted CVD methods.[39,40] However, the synthesis of these diamond nanowires has proven to occur with a low probability and be very difficult to reproduce, despite the many attempts we and others have made, and despite the their potential applications, such as their highly efficient single-photon emission at room temperature[41,42] and high brightness, low-threshold electron-field emission,[40,43–46] as well as for high-performance nano-electromechanical switches[47] and biosensors.[48–54] The RIE method can realize large-scale-oriented nanopillar arrays, but the as-prepared diamond nanopillars have large diameters, usually larger than 50 nm. In addition, the mask materials usually need to be removed. The CVD-based method can achieve smaller crystalline diamond nanowires, but reproducibly synthesizing crystalline diamond nanowires has remained challenging.

This Review is presented with the aim of generating more interest and more effort to address this challenge. We highlight some of the most important synthetic routes that underpin the synthesis of diamond nanowires, then discuss the structures and properties of the diamond nanowires from the reported theoretical and experimental results, and finally, summarize the applications of diamond nanowires.

2. Synthetic Strategies for Diamond Nanowires

2.1. Plasma-Assisted Reactive-Ion Etching

Reactive-ion etching (RIE) is an etching technology used in top-down micro- and nanofabrication. As shown in Figure 1, it uses chemically reactive plasma to remove material deposited on wafers. The plasma is generated under low pressure (vacuum) by an electromagnetic field. High-energy ions from plasma attack the surface of the sample and react with it to form the desired nanostructures. The "output" of plasma etching depends in a nonlinear way on a multitude of adjustable input parameters: power density, frequency, pressure, dc bias, gas composition, flow rate, and so forth. Plasma-based RIE processes offer higher accuracy in replicating device patterns than wet etching patterns, but further advances may depend on a better understanding of gas-phase phenomena and plasma–surface interactions.[55] The first realization of diamond nanowires by RIE was performed by Shiomi, who demonstrated the formation of porous diamond films by oxygen plasma RIE.[28] The plasma-assisted RIE technologies have since been widely developed for the top-down fabrication of diamond nanowires (nanopillars). In the process, a planar nanocrystalline or microcrystalline diamond film is first deposited, and then nanowires or nanorods arrays film are fabricated by the etching of a planar film. Depending on whether a mask is used, the plasma-assisted RIE techniques for diamond nanowires consist of two types, mask-needed and maskless ones.

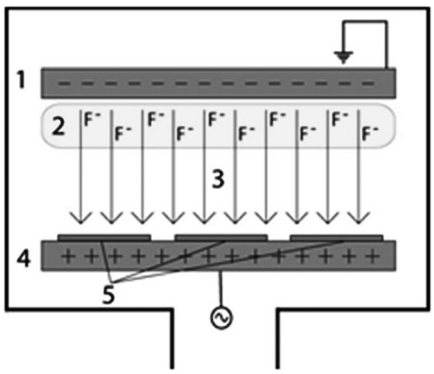

Figure 1. A typical RIE setup, consisting of two electrodes (1 and 4) that create an electric field (3), which can accelerate the ions (2) toward the surface of the samples (5).

2.1.1. RIE Techniques with Masks

Diamond nanowires are generally obtained by the etching of various planar diamond films through various masks including metal nanoparticles, oxide nanoparticles, and diamond nanoparticles. The nanoparticles that are used as masks are a few nanometers in diameter, and the density and the size of the as-prepared diamond nanowires is dependent on the size of the masks.

2.1.1.1. RIE Techniques with Metal Masks

The first realization of diamond nanowires was achieved in 1997 by Shiomi,[28] who demonstrated the formation of a porous diamond film through oxygen plasma RIE by using Al as a mask. Numerous columnar diamond nanowires of approximately 300 nm length and 10 nm width have been made by etching CVD polycrystalline diamond films in O_2 plasma. Ando et al. also reported that diamond nanowires

Yuan Yu received his PhD under the supervision of Prof. Dr. Lian Mao Peng from the Institute of Physics, Chinese Academy of Sciences in 2006. He is currently an assistant professor at the Technical Institute of Physics and Chemistry, Chinese Academy of Sciences. His research interests concern 1D semiconductor nanomaterials, ranging from their synthesis to current applications.

Liangzhuan Wu received his PhD from the Technical Institute of Physics and Chemistry, Chinese Academy of Sciences in 2006. He is currently an assistant professor at the Technical Institute of Physics and Chemistry, Chinese Academy of Sciences. His research interests concern 1D oxides nanomaterials, flexible oxide films, and devices.

with smooth surfaces ($R_a < 0.4$ nm) were obtained by reactive-ion etching in a gas mixture of CF_4 and O_2 by using Al as a mask.[32] The surface roughness (mean roughness of the diamond surface, represented by R_a) of the etched diamond decreased as the CF_4/O_2 ratio increased, although the increase in the CF_4/O_2 ratio reduced the selective etching ratio of diamond versus Al. The gas pressure also affected the surface roughness and the anisotropy of etching. Li and Hatta produced aligned diamond nanowires through radio-frequency (RF) RIE of planar diamond film (obtained by CVD) in an Ar/O_2 plasma in the presence of a patterned Al mask.[56] It was found that diamond whiskers preferentially formed at the diamond grain boundaries. The densities (number of diamond nanowires per unit area) of diamond whiskers increased with the O_2/Ar ratio. A high density of whiskers could be obtained by RF etching with a pure O_2 plasma. The Ar contributed to increasing the etching rate.

The diamond nanowires obtained by Al-masked RIE are polycrystalline, which have the disadvantages of the existence of grain boundaries, impurities, and large stresses in the films. Recently, Liao et al. successfully fabricated single-crystal diamond nanopillars through the Al-masked RIE method,[47] as shown in Figure 2. The fabrication of single-crystal diamond nanowires began from the high-pressure high-temperature (HPHT) type Ib diamond substrate, which

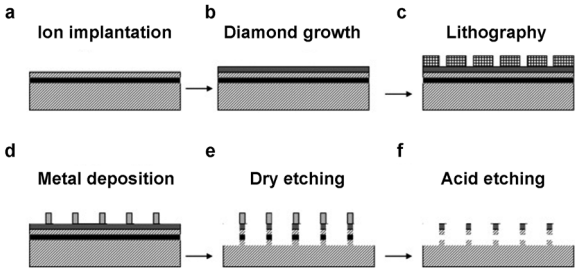

Figure 2. Fabrication of single-crystal diamond nanowires. a) Ion implantation into tybe Ib diamond substrates by carbon ions at an energy of 180 keV and a dosage of 10^{16} cm^{-2}. b) Microwave plasma chemical vapor deposition growth with boron doping (concentration: 10^{18} cm^{-3}). During the growth through chemical vapor deposition, a graphite-like layer with a thickness of around 200 nm was formed below the diamond surface, which acted as the sacrificial layer. c) Electron-beam lithography of the diamond. d) Deposition and lift-off of the aluminum. e) Formation of nanowires by RIE. f) Finally, removal of the Al and graphite by boiling in an acid solution. Reproduced from Ref. [47]. Copyright 2010 John Wiley.

Jinfang Zhi received her PhD under the supervision of Prof. A. Fujishima from the University of Tokyo in 1995. She is currently a professor at the Technical Institute of Physics and Chemistry, Chinese Academy of Sciences. Her research interests concern 1D photoelectric nanomaterials, photocatalytics, and BDD electrochemistry.

was impregnated with carbon ions.[57] A homoepitaxial boron-doped p-type diamond was grown on the substrate by microwave plasma chemical vapor deposition (MPCVD) at 930 °C. After growth, the diamond epilayer was annealed at 900 °C for 3 h in an ultrahigh vacuum (UHV) chamber (base pressure 10^{-7} Pa). A graphite layer with a thickness of 200 nm was formed after the high-temperature processing. Conventional photolithographic and electron-beam lithographic processes were employed to define the cantilevers or bridge structures. An aluminum layer with a thickness of 150 nm was deposited on the patterned diamond epilayer as a mask for reactive-ion etching. The sample was then treated in a boiling acid solution of HNO_3/H_2SO_4 to remove the Al and graphite. Regardless of the implanted ions, high-resolution transmission electron microscopy (HRTEM) images and electron diffraction show that the grown diamond epilayer above the graphite layer still retains a good single-crystal nature, which guarantees that the etched diamond nanowire is of single-crystal structure.

Besides Al, other metals, such as Mo,[33,58] Ni,[34,35] Fe,[59,60] and Au,[61,62] have been successfully used as masks to etch undoped or boron-doped diamond (BBD) nanowires with oxygen plasma. Li and Hatta investigated the effect of the metal masks, including Mo and Ni, on the etched diamond nanowires.[60] It was found that the metal-masked diamond films were distinctly influenced by the oxidizability of the coating metal. Under the same etching conditions, lower density diamond nanowires (10 μm^{-2}) were obtained from the Mo-masked diamond film, while whiskers obtained from the Ni-masked film were more densely distributed (40 μm^{-2}). The authors postulated that oxidizable metals, such as Mo, Fe, and Al, produced metal oxides and metal carbides, which served as a stable coating layer during the etching process and led to the formation of whiskers with lower density. Non-oxidizable metals, such as Ni, which has poor crystallinity and higher mobility in RF plasma etching, did not produce an efficient protecting layer. The distribution of the whiskers might, therefore, be controlled by the type of metal masks. Recently, metal masks of 5–50 nm in diameter were obtained through dewetting various metal films (Al, Ti, Co, Ni, Cu, Pd, Pt, and Au films). Janssen and Gheeraert systematically investigated the effect of the type and thickness of the metal films on the surface density, shape, and size of the resulting metal masks.[63]

2.1.1.2. *RIE Techniques with Oxide Masks*

Fujishima and co-workers reported a technique for the preparation of periodic arrays of diamond nanowires by means of reactive-ion etching with oxygen plasma by using two-dimensional (2D) monodisperse solid SiO_2 particles arrays as masks.[64,65] In a planar diamond surface, fine SiO_2 particle (diameter, 1 μm)[66] are packed in high-density, highly oriented layers (2D periodically arranged SiO_2 particles coating film) over a wide surface area by water evaporation and lateral capillary forces.[67] After preparation of the 2D array, reactive-ion etching (RIE) was carried out with oxygen plasma of the SiO_2 arrays for 5–120 min in a plasma etching apparatus with a radio frequency (RF) generator. Finally, the SiO_2 particles were removed from the diamond with a solution

of HF/HNO_3 (24 wt% HF, 30 wt% HNO_3) to afford the periodic arrays of diamond nanowires. Hausmann et al.[41] have since used oxide nanoparticles, such as SiO_2 and Al_2O_3, as masks in the synthesis of diamond nanowires with both single-crystal and polycrystalline diamond. The authors used inductively coupled plasma (ICP) reactive-ion etching (RIE) with oxygen to fabricate the nanowires. Drop-casted nanoparticles (Au, SiO_2, and Al_2O_3) were used as an etch mask. Al_2O_3 nanoparticles were found to be the most etch resistant. The flowable oxide (Fox, spin-on materials purchased from Dow Corning comprising silicon, carbon, and hydrogen) electron-beam resists (spin-on glass) proved to be suitable etch masks for the fabrication of ordered arrays of diamond nanowires. As shown in Figure 3, single-crystal diamond nanowires with near-vertical side walls were obtained by using Fox as a mask. These well-oriented single-crystal diamond nanowires might be suitable for applications involving quantum information processing.

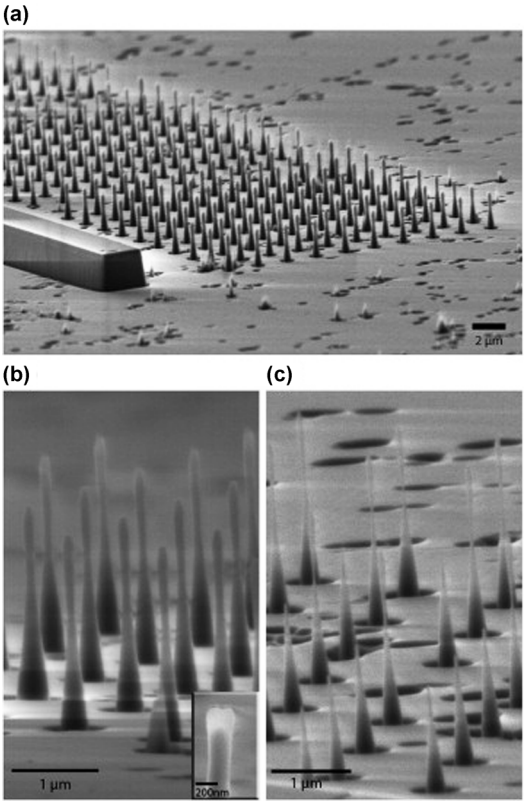

Figure 3. Single-crystal diamond nanowires realized by ICP-RIE. Fox was used to produce an array of pillar-shaped oxide masks with EBL. The mask was then transferred to the substrate by oxygen etching for 10 min and subsequently removed. a) Diamond wires with the same diameters. b) The height of the wires is 2.3 μm from top to bottom. The diameters at the broadest part at the top and the bottom are about 110 nm and 310 nm, respectively. The diameter is about 70 nm at the thinnest part of the nanowires. Inset: one nanowire with the remaining Fox mask after etching. c) An array of nanowires with a height of 2.2 μm high and a bottom diameter of 226 nm. Reproduced from Ref. [41]. Copyright 2010, Elsevier.

2.1.1.3. *RIE Techniques with Diamond Nanoparticles as Masks*

Yang et al. realized vertically aligned diamond nanowires from boron-doped single-crystalline CVD diamond films by using diamond nanoparticles as a mask.[31,68–70] The fabrication process of vertically aligned diamond nanowires is illustrated in Figure 4. First, boron-doped (p-type) diamonds with

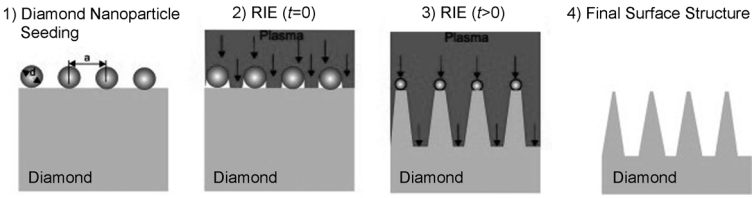

Figure 4. Schematic representations of the fabrication of diamond nanowires. Here, *d* is the diameter of the nanodiamond particles, and *a* is the distance between the particles. Reproduced from Ref. [70]. Copyright 2008 John Wiley.

atomically smooth surfaces are grown by homoepitaxy on Ib diamond substrates by using a microwave-assisted chemical vapor deposition technique.[71] Then, an etching mask made from diamond nanoparticles is deposited. Diamond nanoparticles can be produced with a well-defined size and quality.[72] The diamond nanoparticles of about 8–10 nm in diameter are dissolved in water by ultrasonication to form a pseudostable suspension.[73,74] The concentration of this suspension is crucial, and pretreatment of the diamond powder affects the stability of the suspension. The planar diamond film is then immersed into the suspension and sonicated (100 W, 10 min) to seed diamond nanoparticles on the planar surface of the diamond film. The diamond nanoparticle layer is dense and its quality depends on the suspension and sonication time. After deposition of the diamond nanoparticles, RIE in an O_2(97%)/CF_4(3%) gas mixture is typically applied for 2 to 60 s. Vertically aligned diamond nanowires arise where diamond nanoparticles have been deposited. The as-fabricated diamond nanowires were biofunctionalizated and used for DNA sensing.[69,70]

2.1.2. *Maskless RIE Techniques for Highly Doped Diamond Nanowires*

As mentioned above, 1D nanostructured diamonds are generally fabricated by etching through various masks, such as anodic alumina, SiO_2 ordered arrays, Au nanodots, molybdenum, nanodiamond particles, and other materials. However, these methods suffer from certain limitations. For example, some masks need be removed by additional chemical or physical processes, or an etching mask needs be intentionally deposited by pre-preparation processes. Moreover, the mask-etched diamond nanowires contain some impurities, which usually result from the mask. Finally, the mask-assisted RIE is usually unfavorable for the large-scale fabrication of diamond nanowires. Recently, Fujishima et al. reported a RIE technique for heavily B-doped diamond (BDD) nanowires with a boron doping level of 2.1×10^{21} B cm^{-3} by using oxygen plasma without any additional mask.[75] It is assumed that

boron oxides form on the surface at boron-rich nanometer-sized locations, and they are less volatile than the reaction products, namely, CO and CO_2. In the initial stage of etching, the boron dopant atoms at the diamond surface contribute to the small, nanometer-scale structures. As the etching progresses, the boron species, including oxides, are removed together with carbon atoms, and then they appear to redeposit near the tops of the nanowires and continue to serve as an etching mask. The boron dopant atoms in the diamond act as the mask during plasma etching, thereby avoiding the complicated preparation processes involved in using an intentional mask or removal of the template by additional processes. The formation sites of the nanowire array depend greatly on the boron distribution. Figure 5 shows the SEM

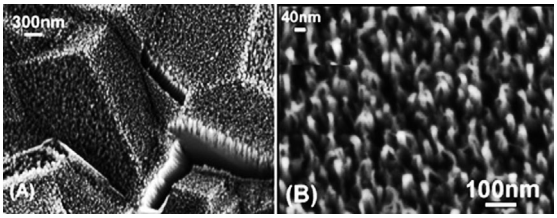

Figure 5. SEM images of a BDD nanowire array at A) low resolution and B) high resolution.

images of the microstructure of a BDD nanowire array. It can be seen that the nanowire arrays on the BDD surface has the following dimensions: 20 nm diameter and 200 nm length, and the distance between each nanograss structure is 50 nm. This straightforward method has the advantage that it does not require any complicated processing steps such as deposition and removal of a mask. This maskless RIE method has been widely used to realize diamond nanowires.[30,76–80]

2.2. Chemical Vapor Deposition (CVD)

Vapor-phase growth is a very useful bottom-up method to produce nanowires. The elemental or oxide nanowires can be achieved through the simple evaporation technique in an appropriate atmosphere.[81–84] The CVD techniques for diamond nanowires consist of two types: template-assisted and template-free ones.

2.2.1. Template-Assisted CVD Methods

Template-assisted CVD synthesis is a convenient and versatile method for generating 1D nanostructures.[85–88] The template uses a pre-existing guide with the desired nanoscale features to direct the formation of nanomaterials into forms that are otherwise difficult to obtain. As a result, template synthesis is capable of producing nanostructures with unique structures, morphologies, and properties. The template serves as a scaffold on which other materials with similar morphologies are synthesized. The in situ generated material is shaped into a nanostructure with a morphology complementary to that of the template. Templates can be nanoscale channels within mesoporous materials, such as porous alumina or polycarbonate membranes.

2.2.1.1. CVD with Nanowire Templates for Diamond Nanowires

One of the most important methods for the synthesis of inorganic nanowires is template-assisted CVD. The semiconductor nanowires derived from noncolloidal synthesis are convenient templates for gas-phase synthesis, including both physical coating as well as chemical transformation. The CVD method with a nanowire template for synthesizing diamond nanowires usually consists of two steps. One is the synthesis of various nanowire templates, and the other is conformal coating of the nanowire templates with nanodiamond-forming polycrystalline diamond nanowires by a CVD method. The size of the as-prepared diamond nanowires is dependent on the size of the nanowire templates. The possibility of depositing layered microdiamond coatings onto tungsten wires by the CVD method was demonstrated for the first time by May.[89] Many others subsequently reported the successful coating of microdiamond onto a variety of substrate wires including silicon carbide, copper, tungsten, and titanium.[90–92] Recently, Singh et al. reported a novel two-step method for the synthesis of high-density nanocrystalline diamond fibers (nanowires). This method includes the synthesis of templates (silica (α-SiO_2) nanofibers) by a conventional vapor-liquid-solid method and the conformal coating of the nanofibers with 15–20 nm sized nanocrystalline diamond (NCD) grains by microwave plasma enhanced chemical vapor deposition under hydrogen-deficient conditions.[93–95] The as-prepared diamond nanowires showed good electron field emission properties.[94,95] Furthermore, our research group also reported a hot-filament chemical vapor deposition method using a Si nanowire template for the fabrication of arrays of boron-doped diamond nanowires and a 2D network of diamond nanowires.[96,97] The synthesis of the arrays of boron-doped diamond nanowires is illustrated in Figure 6.

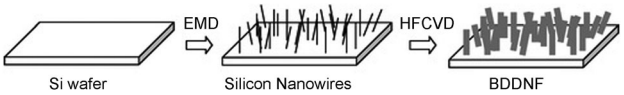

Figure 6. Fabrication of the boron-doped diamond nanowire arrays. Reproduced from Ref. [96]. Copyright 2010, American Chemical Society.

First, silicon nanowires are synthesized by electroless metal deposition (EMD) on a p-type silicon wafer.[98] The substrate is then treated with ultrasound for 20 min in a suspension of diamond nanoparticles. Finally, the BDD nanowires arrays film was prepared by depositing a boron-doped diamond nanocrystal layer onto the as-fabricated Si nanowires (SiNWs) by hot-filament chemical vapor deposition (HFCVD). As shown in Figure 7a, a large number of boron-doped diamond nanorods standing vertically on a silicon wafer can be observed. The inset of Figure 7a clearly shows a single nanorod viewed from the top. The coverage of a nanocrystalline diamond film is complete and continuous

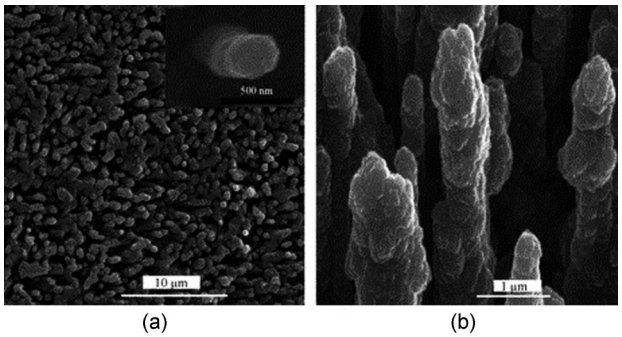

Figure 7. SEM images of the a) top and b) side views of the BDDN. The inset in (a) is an amplified image of a single standing nanowire. Reproduced from Ref. [96]. Copyright 2010, American Chemical Society.

along the whole length (about 5 μm) of the SiNWs. These nanorods possess rough and irregular surfaces with a polycrystalline morphology, as shown in Figure 7b. The as-prepared film of BDD nanowire arrays can be used for the determination of glucose in the presence of ascorbic acid.

2.2.1.2. *AAO-Templated CVD*

Porous anodic aluminum oxide (AAO) templates played a dominant role in the preparation of highly ordered nanowires with controllable size.[99,100] Masuda et al. reported the preparation of well-aligned polycrystalline diamond nanocylinders (nanowires) and diamond-like carbon (DLC) nanotubes on anodic aluminum oxide templates by microwave plasma assisted CVD.[101] The alumina templates[102,103] for diamond deposition were prepared by electrochemical anodization of an aluminum sheet (thickness 0.15 mm) in 0.3 M phosphoric acid at 1 °C under a constant voltage of 190 V for 70 min. The resultant well-ordered holey nanoporous membranes were used as templates for diamond deposition. As shown in Figure 8, prior to deposition, the alumina templates were nucleated with 50 and 5 nm diamond particles for the deposition of diamond nanocylinders and diamond-like nanotubes, respectively. For the growth of nanowire arrays, the 50 nm particles were nucleated at the bottom of the alumina membrane pores with the same diameter (Figure 8a). This enables the growth of diamond cylinders along the length of the pores. For the growth of nanotubes, smaller diamond nanoparticles (5 nm) were ultrasonically dispersed on the pore walls by keeping the templates in suspension (Figure 8b). The growth of the diamond nanowires or nanotubes was carried out by plasma-assisted CVD. The deposition of diamond initially proceeds along the alumina pores and continues to grow on the membrane to yield a continuous film, which acts as a support for the nanostructures. The resulting nanofibers can be released from the alumina membrane by immersion in concentrated phosphoric acid at 250 °C.

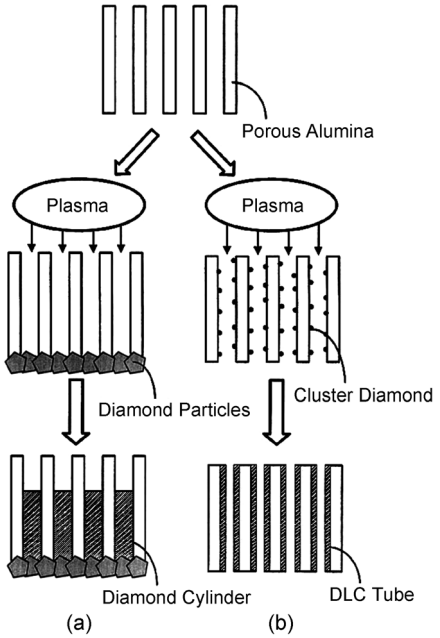

Figure 8. Schematic representation of the fabrication process for cylindrical diamond and tubular structures. a) The cylindrical structures were prepared by nucleating with 50 nm diamond particles at the bottom of the membrane holes, followed by microwave plasma CVD for 3 ± 4 h using acetone as the carbon source. b) Tubular structures were fabricated by nucleating with 5 nm particles on the pore walls of the membrane followed by microwave plasma CVD. Reproduced from Ref. [101]. Copyright 2001, John Wiley.

2.2.2. *Template-Free CVD for Diamond Nanowires*

2.2.2.1. *Microwave Plasma Enhanced CVD*

Valsov et al. reported the microwave plasma-enhanced CVD (MPCVD) synthesis and characterization of new hybrid diamond-graphite nanowires, which were formed on a ultrananocrystalline diamond (UNCD) film.[104] The UNCD films were deposited on Si substrates in a microwave plasma CVD reactor in $Ar/CH_4/H_2/N_2$ mixtures.[105] The cores of the diamond nanowires (DNWs) are 5–6 nm in diameter and grow along the [110] direction. The experimental results showed that N_2 plays an important role in the growth of wirelike diamond grains, which is consistent with the results of Arenal et al.[106] It has been suggested that the low concentration of hydrogen and the introduction of nitrogen into the plasma are two favorable conditions for the synthesis of one-dimensional diamond nanostructures by CVD. A transition from a hydrogen-rich to an argon-rich plasma leads to a decrease in the stability of the diamond phase from the macro- to the nanoscale.[107] Theoretical models suggest that nanocrystalline diamond may be structurally stable both in quasi-zero-dimensional (nanograin)[108,109] and in one-dimensional nanowires.[25,27] However, only the diamond nanograins are observed in UNCD films grown without nitrogen. The high renucleation rate provided by the presence of C_2 dimers in the plasma suppresses the extension of the one-dimensional diamond nanostructures, thereby limiting the grain size within the stability range of the diamond phase, which is about 5 nm.

The introduction of nitrogen in the plasma stimulates the formation of molecular CN species, thus reducing the renucleation rate. This creates favorable conditions for an increase in the grain size and the formation of one-dimensional diamond nanostructures.

Shang et al. reported the growth of ultrathin diamond nanorods (UDNRs) by a MPCVD method (in a N_2/CH_4 plasma).[110] As-deposited UDNRs have a length of 50–300 nm and a diameter of only 2.1 nm, less than the theoretical minimum value (2.7 nm) for energetically stable UDNRs.[25,27] The growth of UDNRs has been suggested to follow a heterogeneous self-catalytic vapor-liquid mechanism. Together with diamond nanoclusters and multilayer graphene nanowires/nano-onions, UDNRs are self-assembled into isolated electron-emitting spherules and exhibit a field emission performance with a low threshold and a high current density (flat panel display threshold: $10\,mA\,cm^{-2}$ at $2.9\,V\,\mu m^{-1}$). Recently, Sobia et al. reported the effect of nitrogen on the incorporation of hydrogen in thin films of diamond nanorods obtained by the MPCVD method (in $Ar/H_2/CH_4/N_2$ plasma). The results showed that the addition of nitrogen to the gas phase increases the non-diamond content in the films.[111] The incorporation of hydrogen in the diamond nanowires was found to increase as the nitrogen in the feed gases in the deposition chamber was increased. Raman spectroscopy measurements show that the increase in the incorporated amount of hydrogen is related to the low crystallinity of the film arising from the increase in the non-diamond content in the samples. More recently, Shalini et al. reported the synthesis of diamond nanowire films by MPCVD (in $Ar\text{-}N_2/CH_4$ plasma).[112,113] The experimental results showed that the electrical conductivity and the fraction of sp^2 bonding in the grain boundary of the diamond nanowire film (π states) increased proportionally with the amount of nitrogen incorporated.[112] They used the diamond nanowire films generated by N_2-rich MPCVD (6% CH_4/94% N_2) as an electrode to detect dopamine.

In conclusion, N_2 plays an important role in the growth of wirelike diamond grains during the DNW growth process by MPCVD. The introduction of nitrogen into the plasma stimulates the formation of molecular CN species, thereby reducing the renucleation rate provided by the presence of C_2 dimers in the plasma and creating favorable conditions for an increase in the grain size and the formation of one-dimensional diamond nanostructures. In addition, the incorporation of hydrogen in the diamond nanowires was found to increase as the nitrogen in the feed gases in the deposition chamber was increased. This leads to the fraction of sp^2 bonding in the diamond nanowire film grain boundaries (π states) increasing proportionally with the amount of nitrogen incorporated, since the hydrogen incorporated into the DNWs can lower the crystalline quality of the DNWs. Therefore, DNWs with an MPCVD-induced high incorporation of N_2 usually display good electrochemical properties, which is accounted for by the increase in the sp^2 content, new C–N bonds at the diamond grains, and an increase in the electrical conductivity at the diamond grain boundaries.[113]

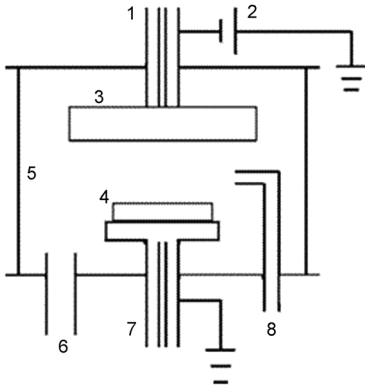

Figure 9. Schematic representation of a HCDC-PCVD device: 1. cathode, water-cooled unit; 2. dc power supply; 3. cathode; 4. anode; 5. water-cooled vacuum chamber; 6. outlet to pump; 7. water-cooled substrate holder; 8. inlet of resource gases.

2.2.2.2. *Hot Cathode Direct Current Plasma Chemical Vapor Deposition (HCDC-PCVD)*

hot cathode direct current plasma chemical vapor deposition (HCDC-PCVD) is an effective method for the deposition of diamond films (including nanocrystalline and microcrystalline diamond films), and diamond films can be deposited uniformly over a large area and with a high growth rate. A schematic diagram of the nonpulsed hot cathode dc-PCVD apparatus is shown in Figure 9. The cathode is made from a tantalum disc and is connected to a water-cooled cylindrical copper block. The anode, on which the substrate lies, is a water-cooled copper block, and a hot cathode and a nonpulsed-type dc power source are used. A long-time stable glow discharge at a large discharge current and a high gas pressure has been used to fabricate high-quality diamond films by using a hot cathode in the temperature range 800–1500 °C and a nonsymmetrical conguration of the poles, in which the diameter of the cathode is larger than that of anode. Nanocrystalline diamond films with different grain size, surface smoothness, and quality have been prepared on Si substrates by changing the composition of the $CH_4/Ar/H_2$ gas mixture.[114] HCDC-PCVD is an effective method for the deposition of diamond films over a large area and with a high growth rate. Zeng et al. reported that (111) diamond microcrystals and (100) diamond microcrystals and nanorods were synthesized on Si substrates by HCDC-PCVD in a CH_4/H_2 gas mixture.[115] The results showed that a high temperature (1223 K) and low CH_4 concentration led to the growth of (111) microcrystalline diamond films, but a low temperature (1098 K) and high CH_4 concentration can lead to the growth of (100) diamond microcrystals and nanorods. Furthermore, the low reactor temperature and high CH_4 concentration decreased the grain sizes, purity, and quality of the diamond films, but increased the transmittance of the diamond films.

2.2.2.3. Catalyst-Assisted Atmospheric-Pressure Chemical Vapor Deposition

Techniques for growing crystalline diamond have evolved from the high-temperature high-pressure (HTHP) method[116] to plasma-enhanced chemical vapor deposition (PECVD) techniques.[112,113] Diamond microwires with a diameter of 25 μm and a length of 400 μm were synthesized in 1968 by using a radiation heating unit developed from a super-high-pressure xenon tube.[117] However, the fabrication of long, single-crystalline diamond nanowires by conventional thermal CVD methods has so far proven elusive, despite the potential benefits. In 2010, however, Hsu et al. synthesized, by chance, diamond nanowires by a chemical vapor deposition method at atmospheric pressure without plasma or energy radiation being used during the CVD.[39] The growth process began with the flow of methane and hydrogen over the Fe catalyst solution dispersed on a silicon substrate under conventional CVD conditions at 900 °C. After this process was completed, and without pumping the residual methane from the chamber, pure hydrogen was flowed through the quartz tube chamber at a rate of 200 sccm while the temperature was slowly lowered to ambient at a rate of about 1.2 °C min^{-1} over a period of 12 h. As shown in Figure 10 A and Figure 10 B, the as-prepared diamonds were straight, thin, and long, and with a longitudinally uniform exterior diameter (60–90 nm) along the entire lengths of tens of micrometers. The structure of the nanowire consists of a diamond core encased within a graphitic shell. The HRTEM image (Figure 10 C) of one of these nanowires reveals a crystalline diamond wire structure with a lattice constant of 0.21 nm, which corresponds to the (111) orientation of diamond. Hydrogen plays an important role in the formation of the diamond nanowires since it can facilitate the transformation of bonds involving sp- and sp^2-hybridized into bonds involving sp^3-hybridized atoms.[118] When the final step of cooling under a hydrogen flow was omitted, carbon nanotubes and amorphous carbon were synthesized, but no diamond nanowires were evident. Transition metals (Fe in this experiment) are now known to facilitate the dissociation of hydrogen molecules into atomic hydrogen with a significantly low energy barrier.[119,120] Atomic hydrogen was demonstrated to enhance diamond nucleation as well as graphite etching, and thus has been widely used for the growth of synthetic diamonds. The authors summarized their achievement in a minireview, and gave a possible mechanism for the formation of the diamond nanowires.[40] They rationalized that the growth of the diamond nanowires begins with the conventional synthesis of either a diamond stud or graphitic tubes through a vapor-liquid-solid (VLS) process, which is then followed by the in situ nucleation and growth of diamond wires, fueled by the subsequent flow of hydrogen in the presence of a solid and gaseous carbon feedstock.

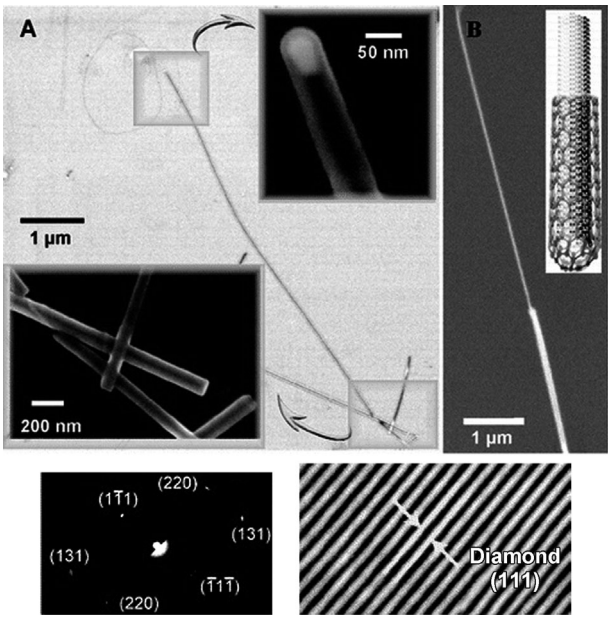

Figure 10. A) Electron microscopy of diamond nanowires encased within a carbon nanotube shell. The diamond core is enclosed in a CNT sheath and is typically tens of micrometers in length and 60–90 nm in exterior diameter. B) An SEM micrograph showing laser stripping of a portion of the graphitic shell of a CVD-grown core–shell diamond nanowire. C) High-resolution transmission electron microscopy (HRTEM) images and selective-area electron diffraction (SAED) pattern of a single diamond nanowire, indicating a crystalline cubic diamond (c-diamond) structure. Reproduced from Ref. [39]. Copyright 2010, American Chemical Society.

2.3. Diamond Nanowires Generated from sp^2-Hybridized Carbon and sp^3-Hybridized Diamondoids

The transformation of graphite to diamond nanocrystals has been one of the most challenging problems in material science for many decades. In general, high pressures and high temperatures are needed to induce this transformation, and catalysts are used to increase the yield of diamond. Research has revealed that carbon nanotubes could also transform into diamond nanocrystals under different processing conditions—laser-induced transformation,[121] chemical vapor deposition by coating of nanotubes,[122] shock waves,[123] and direct transformation under high pressures and high temperatures (HPHT).[124–126] The mechanism of the transformation of carbon nanotubes into diamond was proposed to be nanotubes to carbon onions to diamond.[127] The last step was identified to be critical in the nucleation and growth of diamond nanocrystals in the centers of spherical carbon onions under intense electron irradiation at high temperatures. However, transferring sp^2-hybridized carbon to 1D diamond nanowires is still challenging.

2.3.1. Post-Treatment of Multiwalled Carbon Nanotubes (MWCNTs) with Hydrogen Plasma

Sun et al. described a simple way for transforming CNTs into nanocrystalline diamond, that is, by a hydrogen plasma induced structural transformation.[128] Diamond nanowires with diameters of 4–8 nm and with lengths up to several hundreds of nanometers were obtained simply by prolonging the time of the hydrogen plasma treatment.[36,37] The high-magnification TEM image (Figure 11) shows that the nano-

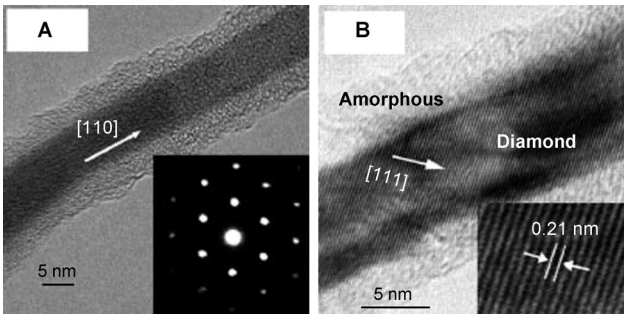

Figure 11. A) High-magnification TEM image of the nanowires showing the core–sheath structure, with the core being the diamond nanowire. The inset shows the SAED along the [111] zone axis perpendicular to the nanowire growth direction. B) HRTEM image of the crystalline-diamond core and amorphous-carbon sheath. The inset shows the (111) planes with a spacing of 0.21 nm. Reproduced from Ref. [37]. Copyright 2013, John Wiley.

wires form a core-sheath structure. A vapor-liquid-solid (VLS) growth mechanism of 1D nanomaterials seems to be unlikely for the growth of these diamond nanowires, since no metal catalysts are used in the synthesis process. The authors proposed a three-step process for the formation and growth of diamonds under the treatment of MWCNTs with hydrogen plasma, including clustering, crystallization, growth, and faceting, which is similar to that proposed by Singh for the nucleation, crystallization, and growth of diamonds from amorphous carbon precursors.[129] Figure 12 shows the proposed model for the formation of nanodiamonds and the growth of diamond nanowires. Amorphous carbon clusters are formed in step I. The crystallization of diamond then begins in the core of the carbon clusters (step II), which is followed by the diamond growth and faceting stage (step III). After the diamond nanocrystallites are faceted, diamond nanowires begin to grow at the nanowire tips (step IV). The amorphous carbon layers that form a sheath around both the diamond nanoparticles and nanowires are important for the 1D growth of diamond nanowires, as they prevent the lateral growth of the diamonds and provide the carbon source for the growth of diamond nanowires.

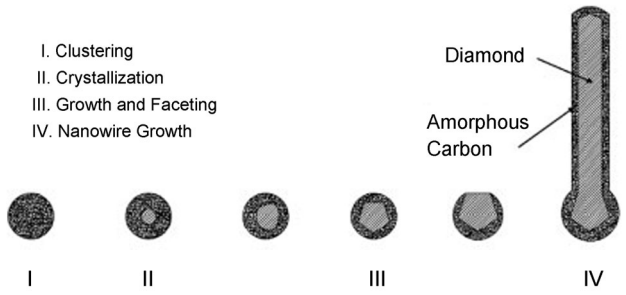

Figure 12. Proposed model for the formation of nanodiamonds, and the growth of diamond nanowires by irradiation of multiwalled carbon nanotubes with hydrogen plasma at high temperatures. Reproduced from Ref. [37]. Copyright 2013, John Wiley.

2.3.2. *Diamond Nanowires Grown from Fullerenes*

Dubrovinskaia et al. reported the synthesis of a bulk sample of nanocrystalline cubic diamond with crystallite sizes of 5–12 nm from fullerene (C_{60}) at 20 Gpa and 2000 °C by using a multi-anvil apparatus.[130] The new material is at least as hard as single-crystalline diamond. It was found that nanocrystalline diamond at high temperature and ambient pressure is kinetically more stable with respect to graphitization than usual diamond. Almost simultaneously, they synthesized aggregated diamond nanorods (ADNRs) from C_{60} at 20(1) GPa and 2200 °C by using a multi-anvil apparatus.[38] The individual diamond nanorods have a diameter of 5–20 nm and are longer than 1 μm. The measured density of the ADNRs was about 0.2–0.4 % higher than that of usual diamond.

2.3.3. *Diamond Nanowires from Diamonoids*

Diamondoids have been found to have strong affinity towards compatible host structures, such as cyclodextrins[131] and CNTs.[132] Analogous to the fabrication of 1D sp^2-hybridized CNTs from 0D sp^2-hybridized fullerenes,[133,134] diamondoids may also fuse and transform into 1D sp^3-hybridized diamond nanowires. The templated growth of these nanowires from 1D diamondoid aggregates confined in CNTs provides a possible pathway through a "face-fused" reaction. However, the fusion reaction of adamantane into diamond nanowires has been shown to be energetically unfavorable.[109] Zhang et al. presented theoretical and experimental evidence for the feasibility of a fusion reaction of diamantane-4,9-dicarboxylic acid, a diamondoid derivative containing relatively reactive functional groups, to 1D diamond nanowires inside CNTs.[135] The diamondoid diacid is more reactive than the pristine diamondoid, and thus requires milder reaction conditions. Unlike in 3D space, the diamantine dicarboxylic acid molecules are pulled inside a CNT by an effective "capillary force" that originates from the stabilization of the molecule inside the surrounding nanotube. The fusion of diamantane-4,9-dicarboxylic acid under the confinement of CNTs may be a promising way to generate diamond nanowires. The diamantane-4,9-dicarboxylic acid was sublimed and self-assembled into the quasi-1D space of double-wall CNTs (DWCNTs) by a vapor-phase reaction. Since the sublimation temperature of the diamantane-4,9-dicarboxylic acid was 300 °C in air atmosphere, an encapsulation temperature of 280 °C at 10^{-6} Torr was chosen. Similar to adamantane, the encapsulation of diamantane-4,9-dicarboxylic acid is highly selective with respect to the inner diameter (D_{inner}) of the CNT. There is no encapsulated diamantane-4,9-dicarboxylic acid in DWCNTs which have $D_{inner} < 0.8$ nm (Figure 13a). However, the diamantane-4,9-dicarboxylic acid aligned well along the axis of DWCNTs with compatible $D_{inner} \approx 1.0$ nm (Figure 13b), which is consistent with computational results for the encapsulation of diamondoids.[136] Multiple arrays of encapsulated molecules can often be found in CNTs with much wider D_{inner} values (Figure 13c). As demonstrated by the formation of diamond by chemical vapor deposition (CVD)[137] and the thermal annealing of

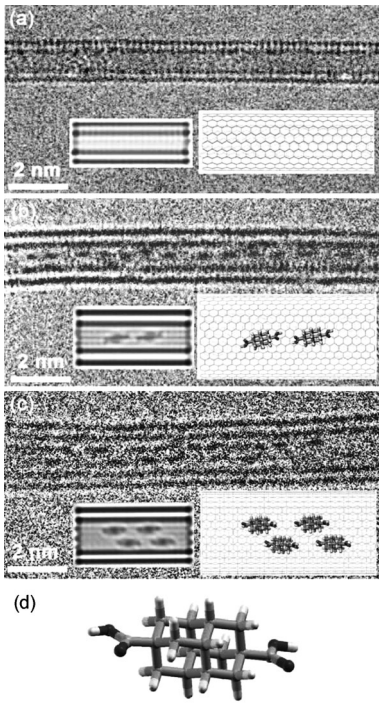

Figure 13. HRTEM and simulated images as well as model structures of a) empty DWCNTs ($D_{inner} < 0.8$ nm), b) linear diamondoid arrays inside DWCNTs ($D_{inner} \approx 1$ nm), c) multiple diamondoid arrays inside DWCNTs ($D_{inner} \approx 1.3$ nm), and d) optimized structure of the diamantane-4,9-dicarboxylic acid molecule. Reproduced from Ref. [135]. Copyright 2013, John Wiley.

adamantane inside CNTs,[132] hydrogen plays a crucial role in retaining the sp^3-hybridized diamond cages. The as-produced diamondoid 1D aggregates in DWCNTs were annealed at 600 °C for 12 h under a flow of hydrogen. Diamond nanowires (DNWs) were then found inside DWCNTs with $D_{inner} \approx 1.3$ nm. The rod-shaped product has a diameter of about 0.78 nm, and it is very stiff and straight. No nanowire structures have been observed in DWCNTs with a smaller D_{inner} value of around 1.0 nm.

In conclusion, numerous efforts have been directed at developing various synthetic methods to prepare diamond nanowires, including reactive-ion etching (RIE), plasma post-treatment of carbon nanotubes, transformation of fullerene to diamond nanowires at high temperature and high pressure, as well as template- or catalyst-assisted CVD method. Diamond nanopillars obtained from RIE maintain the structural features of the planar diamond matrix. The RIE method can lead to large-scale oriented nanopillar arrays, but the as-prepared diamond nanopillars have a large diameter, usually larger than 50 nm. In addition, the mask materials usually need to be removed. The CVD-based method can achieve smaller crystalline diamond nanowires, but reproducibly synthesizing the crystalline diamond nanowires is still challenging.

3. Structures and Properties: Simulations and Experiments

3.1. Structural Stability of Diamond Nanowires

Diamond-based materials have been suggested to be the optimal choice for nanomechanical applications because of their high elastic modulus and strength-to-weight ratio.[140] This has prompted a number of theoretical studies on various properties of diamond on the nanoscale. The results of these investigations have shown that dehydrogenated C(111) octahedral nanodiamond surfaces are structurally unstable, with their presence inducing phase transitions from the sp^3 structure of nanodiamonds to the sp^2 structure of carbon onions. However, the presence of cubic surface facets has been found to promote stability. For example, whereas cuboctahedral nanodiamond structures have exhibited preferential exfoliation of C(111) surfaces over lower-index surfaces, increasing the C(100) surface area produces a more stable nanodiamond structure and reduced surface graphitization.

Although the sp^2 bonding of carbon nanotubes (CNTs) offers many structural advantages, the smallest nanotubular structure has been predicted to possess sp^3 bonding,[138] as sp^2 bonding appears to be unfavorable.[139] Only a few diamond nanowire structures have been observed experimentally, which raises questions as to the phase stability of one-dimensional diamond structures (nanowires or nanorods). If diamond is to play a significant role in the future of nanodevices, it is important to gain a full understanding of the phase stability of dehydrogenated diamond nanowires and carbon nanotubes, to determine if diamond nanowires are energetically favorable compared to carbon nanotubes. Barnard et al. studied the structural properties of dehydrogenated diamond nanowires using the Vienna ab initio simulation package (VASP).[25] Three kinds of diamond wires, dodecahedral, cubic, and cylindrical nanowires, were considered. The dodecahedral structures are bound by (110) surfaces in all lateral directions, with a square cross-section, and have a principal axis in the [100] direction. The cubic diamond nanowires are bound by two C(100) surfaces and two C(110) surfaces in the lateral directions, with a rectangular cross-section, and have a principal axis in the [110] direction. Finally, the three cylindrical nanowires considered in the study are bound by two C(100) surfaces and two C(110) surfaces in the lateral directions, with a circular cross-section, and have a principal axis in the [100] direction. Changes in the energy per atom (ΔE), cross-sectional area (ΔA), and nanowire segment lengths (ΔL) resulting from the relaxation of the morphology of each nanowire are shown in Table 1. The structural changes ΔA and ΔL are also shown in terms of the percentage change in Figure 14. In theory, each plot in Figure 14 should converge to zero as the number of atoms increases (the macroscopic limit), but there are too few data points to deduce anything but the overall trend. The smallest cubic nanowire has been excluded from this comparison because of its conversion into a nonclassical nanotube. It is apparent from Table 1 that the remaining cubic nanowires still exhibit unusual structural changes. The slopes for the

Table 1: Changes in energy per atom (ΔE), cross-sectional area (ΔA), and nanowire segment lengths (ΔL) resulting from the relaxation of the morphology of each nanowire.[25]

Morphology	Atmos	ΔE [eV]	ΔL [nm]	ΔA [nm^2]
dodecahedral	75	−0.2271	+0.0883	−0.0428
dodecahedral	144	−0.2150	+0.1051	−0.0578
dodecahedral	196	−0.2057	+0.0722	−0.0586
cubic[a]	84	−0.9812	−0.0222	
cubic	132	−0.4847	−0.0094	−0.0265
cubic	240	−0.4339	−0.0038	−0.0615
cylindrical	63	−0.7063	+0.0199	−0.0336
cylindrical	128	−0.5687	+0.0182	−0.0421
cylindrical	228	−0.2676	+0.0017	−0.0448

[a] Nonclassical nanotube.

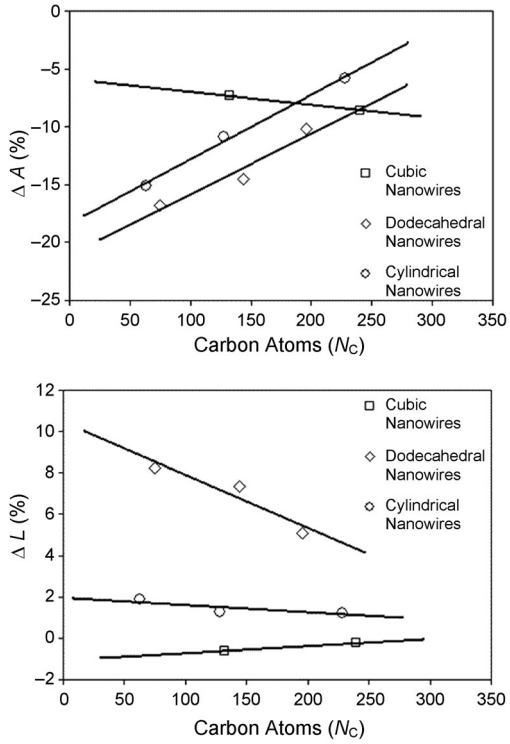

Figure 14. Percentage change in the cross-sectional area ΔA (top) and in the periodic segment length ΔL (bottom) for the respective morphologies. Reproduced from Ref. [25]. Copyright 2003, American Chemical Society.

cubic nanowires are positive, whereas the slopes for the cylindrical and dodecahedral nanowires are negative. This is thought to be a product of the cubic nanowire having a principal axis in the [110] direction, and suggests that this is not an optimal choice for diamond nanowire structures. It has been shown from the ab initio relaxation of diamond nanowires that nanocrystalline diamond may be structurally stable in one dimension. Diamond nanowires with dodecahedral and cubododecahedral morphology retained the diamond structure upon relaxation, but did exhibit significant relaxation involving changes in the length and cross-sectional area. The stability, characterized by the variation in these structural properties from that of bulk diamond, has been found to be dependent on both the surface morphology and the crystallographic direction of the principal axis of the nanowire. For example, nanowires having a principal axis in the [110] direction do not represent an optimal choice for diamond nanowire structures. Although all the structures under consideration exhibited significant changes in the length and cross-sectional area, dodecahedral diamond nanowires with their principal axis in the [110] direction appear less structurally favorable.

Barnard et al. presented a theoretical investigation of the relative phase stability of 1D carbon nanostructures, including carbon nanotubes and diamond nanowires, based on a heat of formation model previously used successfully to compare the phase stability of diamond nanocrystals and fullerenes.[27] The results of this study indicate that carbon nanotubes represent the most energetically preferred form of fine 1D carbon nanostructures, and the diamond nanowires occupy a "window" of stability. This window ranges from approximately 2.7 nm to 3.7–9 nm in (lateral) diameter, beyond which graphite is energetically preferred. The limits of this range are sensitive both to the nanowire morphology, and the method used to scale the graphite structures (required to ensure dimensional consistency). These results are considered to be useful in estimating the size range for which diamond nanowires may be expected during synthesis, and as a guide to the relative stability of sp^2- and sp^3-hybridized carbon atoms in 1D nanostructures.

Tanskanen et al. studied the structural stability of the polyicosahedral diamond nanowires obtained from icosahedral diamondoids and conventional diamond nanowires that are superimposable with bulk diamond.[141] The molecular structures of three icosahedral diamondoids, $C_{20}H_{20}$, $C_{20}@C_{80}H_{60}$, and $C_{20}@C_{80}@C_{180}H_{120}$, together with the corresponding polyicosahedral diamond nanowires are illustrated in Figure 15. The B3LYP-calculated energetics, HOMO–LUMO gaps, and band gaps are summarized in Table 2. The strain energies suggest the 1D diamond nanowires (DNWs) to be favored over the dodecahedral $C_{20}H_{20}$. The low structural strain of the DNWs derived from dodecahedrane is in agreement with previous studies on short oligomers of dodecahedrane.[142,143] To take the effect of thermodynamics into account, the authors calculated the Gibbs-corrected strain energies at $T = 298.15$ K for dodecahedrane and its 1D counterparts. The Gibbs corrections show the dodecahedrane to be slightly favored over its 1D counterparts. The differences are small, however, which suggests the polyicosahedral DNWs are thermodynamically viable. With the exclusion of dodecahedrane, the strain energies increase, but only slightly, as a function of the length of the polyicosahedral diamondoid, thus suggesting the preference for icosahedral structures. Combining the icosahedral diamondoids with polyicosahedral DNRs reduces the number of strain-inducing pentagons. However, connecting the cages introduces additional strain to the interface region through fused pentagons. Nevertheless, the strain energies are systematically lower for the polyicosahedral DNRs than for the experimentally known dodecahedrane. The relative proportion of the fused pentagons becomes lower as a function of the diameter, thereby decreasing the strain energies of the polyicosahedral DNRs

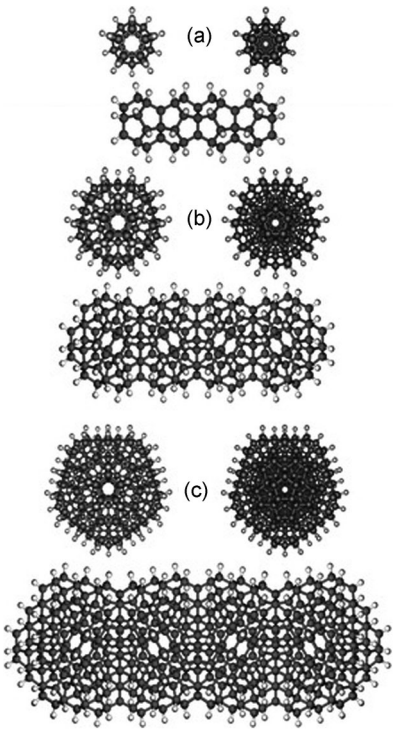

Figure 15. Icosahedral diamondoids (top left) and their polyicosahedral diamond nanowires (top right and bottom): a) $C_{20}H_{20}$, b) $C_{20}@C_{80}H_{60}$, and c) $C_{20}@C_{80}@C_{180}H_{120}$. Reproduced from Ref. [141]. Copyright 2008, American Chemical Society.

Table 2: Dimensions, strain energies, and HOMO–LUMO band gaps of the icosahedral diamondoids and their 1D counterparts.[41]

Stoichiometry	No. of combined cages	Diameter [nm]	Length [nm]	ΔE	Band gap [eV]
$C_{20}H_{20}$	1	0.66	0.66	14.6	8.49
$C_{35}H_{30}$	2	0.64	0.87	13.8	8.26
$C_{65}H_{50}$	4	0.64	1.56	13.2	8.14
$C_{125}H_{90}$	8	0.64	2.59	13.0	8.05
$C_{30}H_{20}$	∞	0.64	∞	12.8	8.01
$C_{20}@C_{80}H_{60}$	1	1.09	1.09	8.3	7.39
$C_{175}H_{90}$	2	1.09	1.59	8.7	7.26
$C_{325}H_{150}$	4	1.09	2.56	9.0	7.14
$C_{625}H_{270}$	8	1.09	5.04	9.1	7.11
$C_{150}H_{60}$	∞	1.09	∞	9.4	7.13
$C_{20}@C_{80}@C_{180}H_{120}$	1	1.52	1.52	6.3	7.01
$C_{490}H_{180}$	2	1.53	2.31	7.0	6.81
$C_{910}H_{300}$	4	1.53	3.92	7.5	6.68
$C_{280}H_{120}$	∞	1.53	∞	8.2	6.65
$C_{80}H_{20}@C_{180}H_{120}$	1	1.52	1.52	7.9	6.43
$C_{450}H_{220}$	2	1.52	2.30	8.7	6.04
$C_{830}H_{380}$	4	1.52	3.89	9.2	5.87
$C_{380}H_{160}$	∞	1.53	∞	9.9	5.75

derived from the larger icosahedral diamondoids. Comparisons between the 1D diamond nanowires of $C_{20}@C_{80}@C_{180}H_{120}$ and the corresponding hollow $C_{80}H_{20}@C_{180}H_{120}$ show the filled structures to be energetically favored.

Representative examples of the hydrogenated conventional DNWs, namely, DNWs that are superimposable with bulk diamond, have been investigated. The calculated strain energies are clearly the lowest for those conventional DNWs whose principal axes are parallel to the [110] direction of bulk diamond. The highest stability of the [110] DNWs can be understood to originate from surface hydrogenation. The H-H distance between the surface hydrogen atoms is around 2.5 Å for the [110] DNWs, but only 2.0 Å for the [100] and [111] DNWs. The repulsion between the surface hydrogen atoms thus somewhat destabilizes the [100] and [111] DNWs, whereas the repulsion is negligible for the [110] DNWs. The described preference for hydrogenated [110] DNWs has also been observed experimentally, with DNRs synthesized by post-treatment of multiwalled CNTs with hydrogen plasma preferring the [110] growth direction.[34] Previously, dehydrogenated DNWs had been shown to prefer structures with their principal axis parallel to the [100] direction, while [110] DNWs had been reported to be unstable.[25,26] As a consequence of the impact of H-H interactions at the surface, the presence (or absence) of hydrogen in the synthesis of DNWs and DNRs may have an effect on the orientation of the products.

3.2. Mechanical Properties of Diamond Nanowires

With its exceedingly high bulk modulus and hardness, diamond has historically been considered the strongest material. Recently, however, it has been claimed on the basis of both theory and experiment that carbon nanotubes are both stiffer and stronger along their axis than diamond. A problem with this claim is that it is difficult to make a fair comparison between these two representatives from the macro- and nanoscales unless some additional assumptions about their structure are made, for example, an effective "thickness" of a sheet of carbon atoms comprising a nanotube. Shenderova et al. compared the stiffness and fracture force of hydrogenated diamond nanorods with those of single-walled (SWNTs) and multiwalled carbon nanotubes (MWNTs).[24] It was determined that the mechanical properties of the nanorods depend on both the diameter of the nanorod and the orientation of the principal axis. The general analysis suggests that while a SWNT has a higher strength-to-weight ratio, above a critical radius between about 1 and 3 nm (depending on the DNR structure) the force needed for brittle fracture of a DNR exceeds that of a SWNT. This higher fracture force results from the larger load-bearing cross-sectional area of DNRs compared to SWNTs at the same diameter. Similarly, the calculations show that the zero-strain stiffness of DNRs will exceed that of SWNTs for radii greater than about 1 nm. Two additional important factors to consider when comparing the mechanical properties of SWNTs and DNRs are their relative compactness and strength-to-weight ratios. The calculated results clearly show that DNRs are more compact than SWNTs, and therefore a DNR would in general displace less volume in a nanocomposite than a comparable SWNT. To illustrate the relative strength-to-weight ratios of DNRs and SWNTs, the ratio between the diameter of a DNR and

a SWNT as a function of the nanotube diameter was calculated by the authors for two cases, under the condition of equal fracture force and under the condition that the two structures being compared were of equal weight. Under the equal fracture force condition, the DNR/SWNT weight ratio for the two structures is constant at 1.47:1. When the diameters are smaller than the critical diameter, DNRs require a larger diameter to bear the same load as the corresponding SWNT. Under the requirement of equal weight, the ratio between the related fracture forces for the DNR/SWNT is 0.68:1. At larger diameters, DNRs are therefore stronger, but at the cost of a lower strength-to-weight ratio. Similar to the strength analysis above, the stiffness of DNRs and SWNTs was compared by the authors. The calculated results show that $<001>$ and $<111>$ DNRs are stiffer than SWNTs at diameters exceeding about 1 nm.

The results above establish that DNRs are important target structures for synthesis. To explore whether DNRs are viable target structures, the authors used molecular modeling studies to characterize the binding energies of several examples of DNR structures. For large carbon-to-hydrogen ratios, the DNRs and the SWNTs are roughly comparable in binding energy, while for small ratios the sp^3-bonded structures are energetically favored, in agreement with a previous analysis of carbon-hydrogen clusters.[16]

The mechanical properties of the polyicosahedral and the conventional DNWs, including Poisson's ratios, Young's moduli, and shear moduli, were investigated by Tanskanen et al.[141] For a point of comparison, the elastic properties of a zigzag (22,0) CNT were determined by periodic calculations. The elastic moduli increases as a function of the length of the structure, as is clear from the calculated mechanical properties of $C_{20}H_{20}$ and $C_{20}@C_{80}H_{60}$ cages and their finite 1D counterparts. The Young's moduli increase because the stress caused by distortion from the equilibrium becomes distributed among a larger number of C–C bonds. The increase in shear moduli is due to a larger shear surface.

In general, the Young's and shear moduli follow the same trends. The calculations give the highest Young's modulus for the CNT, included as a reference, a value of about 900 GPa, which is in agreement with previous theoretical and experimental studies.[144] The studied conventional DNWs have Young's moduli around 360–680 GPa, with the moduli increasing as a function of the wire diameter. For approximately the same cross-sectional area of the wire, the [100] DNWs have clearly lower moduli than the [110] and [111] DNWs. At a cross-sectional area of 1.4 nm^2 and greater, the [111] DNWs have the highest Young's moduli of the studied conventional DNWs. This is in agreement with previous calculations, which suggest the [111] direction to have the highest Young's modulus for the low-index orientations of bulk diamond.[38] The Young's moduli of both hydrogenated conventional DNWs and the polyicosahedral DNWs are presented in Figure 16. Similar to the conventional DNWs, the elastic moduli of the polyicosahedral DNWs increase as a function of the cross-sectional area. Furthermore, their Young's moduli are even higher than those of the conventional DNWs. Accordingly, the polyicosahedral DNWs, although being somewhat more strained than the conventional DNWs, could turn out to be valuable in nanomechanical applications.

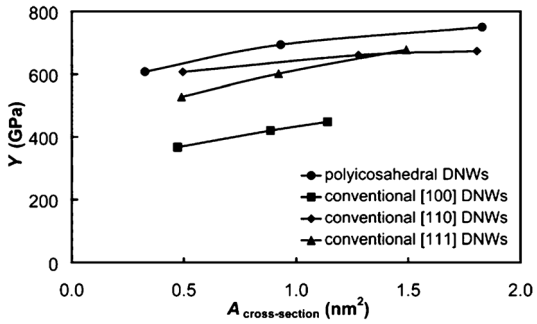

Figure 16. Young's moduli (Y) of the hydrogenated conventional and the polyicosahedral DNWs as a function of the cross-sectional area of the stucture. Reproduced from Ref. [141]. Copyright 2008, American Chemical Society.

Recently, Guo et al. used molecular dynamics simulations to investigate the strain-rate-, temperature-, and size-dependent mechanical properties of [001] orientation diamond nanowires.[145] It was found that, for the same cross-sectional areas, strain rates have almost no effect on the yield strength and Young's modulus, provided the strain rates are within the range of 0.001 to 0.025 ps^{-1}. The calculated results have also indicated that the yield strength, Young's modulus, fracture strength, and fracture strain of diamond nanowires all decrease as the temperature increases from 100 to 500 K. Furthermore, the yield strength, Young's modulus, fracture strength, and fracture strain increase dramatically with increasing cross-sectional area at a temperature of 300 K. The orientation-dependent mechanical properties of diamond nanowires were also studied. Three crystal orientations of DNWs were considered, that is [111], [001], and [011] crystal orientations. The cross-sectional areas of all the DNWs considered here are about 4.58 nm^2. The relationships between the crystal orientations and stress-strain responses for these DNWs with the three crystal orientations are shown in Figure 17. For DNWs with a [001] crystal orientation, the

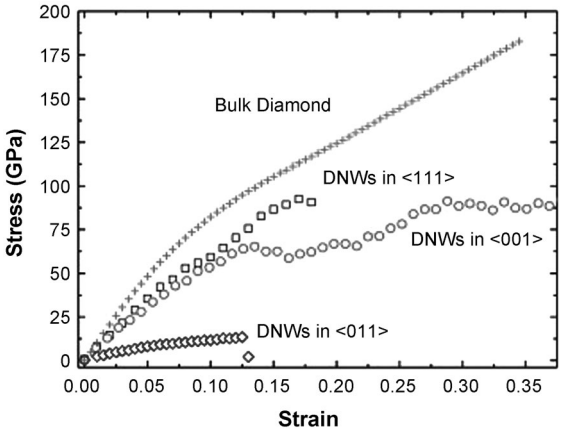

Figure 17. Stress–strain curves of DNWs in the [111], [001], and [011] crystal orientations at 300 K. Also shown are data for bulk diamond computed in this simulation. Reproduced from Ref. [145]. Copyright 2011, Elsevier.

yield strength is 63 GPa and the Young's modulus is 688 GPa. However, for DNWs with a [011] crystal orientation, the Young's modulus falls by 74.7% and the yield strength is 77.8% lower. For DNWs with a [111] crystal orientation, the yield strength is 47.7% greater and the Young's modulus 0.8% larger. In particular, the Young's modulus in the [111] crystal orientation is significantly larger than in the [001] and [011] crystal orientations. It was also found that the Young's moduli of all the studied DNWs were lower than those of bulk diamond.

3.3. Density and Compressibility of Diamond Nanowires

Dubrovinskaia and Dubrovinsky reported the synthesis of aggregated diamond nanorods (ADNRs) from fullerene (C_{60}) at 20(1) GPa and 2200 °C by using a multi-anvil apparatus.[38] Individual aggregated diamond nanorods (ADNRs) have diameters of 5–20 nm and lengths greater than 1 μm. The X-ray density of diamonds with natural abundances of isotopes is 3.515–3.519 $g\,cm^{-3}$. The X-ray density of the material was found to be 3.528(1) $g\,cm^{-3}$, which is about 0.2–0.4% higher than that of usual diamond.[146,147] The samples synthesized in a multi-anvil apparatus have a cylindrical shape that allows their volumes to be determined. The measured density of the bulk ADNR sample was 3.532(5) $g\,cm^{-3}$, in good correspondence with the X-ray data.[146,147] This result is in agreement with theoretical calculations on the structural relaxations of the diamond nanowires.[25] Although the exact crystallographic configuration of individual rods in ADNRs was not theoretically considered in Ref. [25], the main conclusion that the outerlayer contraction, characteristic of diamond nanowires, causes shortening of the C–C bonds may explain the higher density of the ADNRs. Both diamond and ADNRs were compressed simultaneously in Ar to a pressure of over 27 GPa, at which the samples became bridged between the diamond anvils and further compression was not possible. The experimental pressure–volume data were fitted (Figure 18) using the third order Birch–Murnaghan Equation of state.

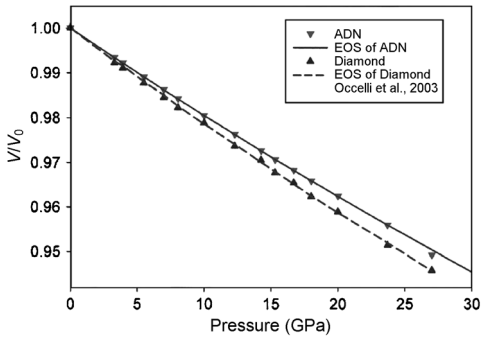

Figure 18. Pressure-dependence of the reduced volume (V/V_0) of diamond (triangles) and aggregate diamond nanorods (inversed triangles). The dashed line shows the third-order Birch–Murnaghan Equation of state (EOS) with parameters $KT = 446(3)$ GPa, $K' = 3.0$, $V_0 = 3.4170(5)$ $cm^3\,mol^{-1}$. The continuous line is the fit to our data with $KT = 491(3)$ GPa, $K' = 3.1(2)$, $V_0 = 3.4014(5)$ $cm^3\,mol^{-1}$. Reproduced from Ref. [38]. Copyright 2005, American Physical Society.

The fitting procedure for diamond gave $KT = 442(4)$ GPa, $K' = 3.2(2)$, and $V_0 = 3.4157(9)$ $cm^3\,mol^{-1}$. For the ADNRs the authors found $KT = 491(3)$ GPa, $K' = 3.1(2)$, and $V_0 = 3.4014(5)$ $cm^3\,mol^{-1}$. Thus, ADNRs are more than 11% less compressible than normal diamond, thus making it an incompressible form of carbon. It also has the lowest experimentally determined compressibility.[148]

3.4. Phonon Optical Mode and Electronic Structure of Diamond Nanowires

The electronic structure of the polyicosahedral diamond nanowires and conventional diamond nanowires were determined by Tanskanen et al. through quantum chemical calculations.[141] As shown in Table 2, the HOMO–LUMO gaps of polyicosahedral diamond nanowires are smaller than those of diamondoids,. The gaps are generally smaller for polyicosahedral diamond nanowires with larger diameters and longer lengths. For conventional diamond nanowires, the band gaps show the same trend as the band gaps calculated for the polyicosahedral DNWs. It is well-known that phonon properties play an important role in the considered systems because of their significance in the analysis of various physical processes, such as charge and thermal transport, and optical transitions, hence the phonon band structures of Si and Ge nanowires have been investigated through DFPT (density functional perturbation theory).[149,150] Recently, a local bond-polarization model based on Green's displacement–displacement function and the Born potential were applied by Trejo et al. to study the confined optical phonons and Raman scattering of diamond nanowires (DNWs).[151] The electronic band structure of DNWs were also investigated by means of a semiempirical tight-binding (TB) approach and compared with density functional theory (DFT) with local density approximation (LDA). The results show that the highest-frequency Raman peak shifts to lower frequencies as the nanowire width increases, as a result of phonon confinement, in accordance with the experimental data.[152] The authors described the electronic properties of H-passivated, free-standing diamond nanowires with widths ranging from 0.25 to 2.52 nm oriented along the [001] direction and contained in the corresponding supercells of 9 to 441 carbon atoms. Figure 19a–d shows the electronic band structure of c-D and DNWs, obtained from TB (blue lines) and DFT-LDA (orange area) calculations. The TB calculations of the electronic band structure of DNWs with $d = 0.50$, 0.37, and 0.25 nm have been shifted by $d = 4.58$, 3.43, and 2.69 eV, respectively to adjust the valence band maximum (VBM) energy to that of the DFT-LDA calculation. It can be seen that the good agreement continues for the VBM but the underestimation of the LDA band gap becomes greater when the size of the DNWs is reduced. It is noteworthy that the DFT-LDA band gap is always direct, while the TB one is indirect in all cases. The difference between the conduction bands could be due to the s* orbital having non-d wave symmetry and additionally because the geometry optimization is absent from the TB calculations. However, in both approaches the band gap shows a clear broadening as a result of quantum confinement.

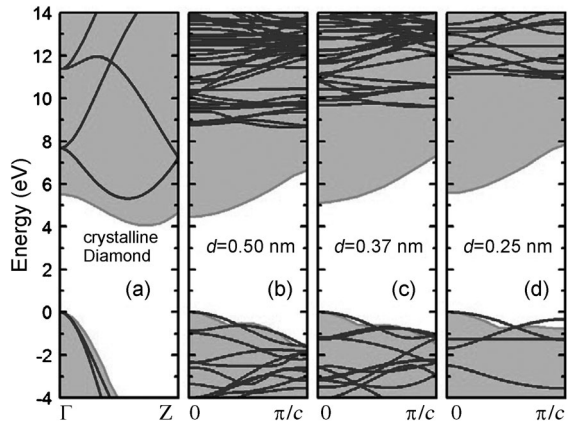

Figure 19. Electronic band structure for: a) c-D and b–d) DNWs calculated from TB (lines) and DFT-LDA (gray area). Reproduced from Ref. [151]. Copyright 2012, Elsevier.

The calculations also showed the almost linear decrease in the band gap as the width of the diamond nanowires is increased, as well as the important contribution of hydrogen atoms to the electronic states around the conduction band minimum (CBM).

3.5. Thermal Conductivity of Diamond Nanowires

In view of the high thermal conductivity of bulk diamond, DNWs may have thermal conductivities that rival CNTs. Moreover, the thermal conductivity of DNWs may be less sensitive to surface functionalization than modeling suggests for CNTs,[153] thereby providing a potentially important mode for enhancing heat transfer within a nanocomposite through cross-linking. On the other hand, the nanometer-scale dimensions of DNWs may severely reduce their thermal conductivity compared to bulk diamond. Experiments and theoretical analysis by Novikov et al.,[154] for example, show that thermal conductivity in polycrystalline diamond thin films is severely reduced as grain sizes approach the nanometer scale as a result of phonon scattering. Moreland et al. used simulations to characterize the thermal conductivity of a (10,10) CNT and a diamond nanowire.[155] They showed that the conductivity of the diamond nanowire is significantly less than that of the CNT, but that the calculated values for the thermal conductivity for both structures depends on the choice of thermostat. Padgett et al. reported thermal conductivity calculations by using classical trajectories of hydrogen-terminated and functionalized DNRs with a [110] long axis, and cross-sectional radii and lengths ranging from 0.578 to 1.606 nm and from 0.016 to 0.128 μm, respectively.[156] The simulations predict that thermal conductivities for DNRs with a hydrogen surface termination are about a factor of 4 less than previously calculated values for pristine (10,10) CNTs. To study the effect of surface functionalization on thermal conductivity, structures have been modeled in which bound phenyl groups replace the surface hydrogen. The simulations indicate that the thermal conductivities of DNRs are much less influenced by surface functionalization than are the thermal conductivities of CNTs, which suggests that DNRs are a viable alternative to CNTs for thermal management in nanocomposites. The simulation results show that the thermal conductivity is strongly dependent on the length and radius of the DNRs for both the hydrogen-terminated and surface-functionalized structures. Guo et al. carried out non-equilibrium molecular dynamics simulations on the geometry- and temperature-dependent thermal conductivities of diamond nanowires.[157] The calculated results indicated that at a temperature of 300 K, the thermal conductivities of the diamond nanowire increases as the length and cross-sectional areas increase. It was also found that the thermal conductivities of the [011] crystal orientation DNWs are larger than those in the [001] and [111] crystal orientation DNWs af the same length, temperature, and cross-sectional area. The thermal conductivities of all the diamond nanowires considered in this study are smaller than those of the corresponding orientations of bulk diamond. Additionally, the thermal conductivities of diamond nanowires in the temperature range 0–1000 K initially increase as the temperature increases, and then decrease. The effects of the geometry and temperature on the thermal conductivities of diamond nanowires can be explained well by the calculated densities of the phonon states.

3.6. Electrochemical Properties of Diamond Nanowires

Planar boron-doped diamond (BDD) electrodes have been recognized as one of the most promising electrode materials and sensing platforms because of the unique physical properties of the diamond film. The diamond interface is chemically stable, exhibits favorable biocompatibility and shows an enlarged potential window together with a low background current relative to other electrode materials such as gold or glassy carbon.[158] Boron-doped diamond (BDD) has been recognized as the best electrode material for electrochemistry, since diamond electrodes have unique features such as a) high chemical stability, b) low tendency for fouling, c) good biocompatibility, d) low background current, and e) wide potential window.[158] The electrochemical background current of BDD in phosphate buffer is 10 times lower than that of a gold electrode and 400 times lower than that of glassy carbon electrode. In addition, boron-doped DNWs, irrespective of whether the nanopillars are obtained by RIE or the nanowires are obtained from CVD, possess better electrochemical properties than planar diamond, although the electrochemical properties of the DNW is dependent on its surface structure and geometrical shape. The working potential window remains wide for the diamond nanopillars and nanowires[31,96,113] in a similar way to the planar BDD electrode, while the redox peak currents of the diamond nanopillars and nanowires are much higher than those on the planar BDD electrode. The redox peak currents of boron-doped diamond nanopillars ($N_A \approx 7 \times 10^{19}$) obtained by using the reactive ion etching method with nanodiamond particles as a hard mask is almost two times larger than that on the planar BDD electrode.[31,70] The enlarged redox peak currents (about 1.8 times) are also observed on boron-doped

diamond nanopillars ($N_A \approx 3 \times 10^{19}$) obtained from maskless RIE compared to the initial planar BDD electrode.[159] Boukherroub and co-workers reported that the boron-doped diamond nanopillar ($N_A \approx 8 \times 10^{19}$) electrode obtained by maskless RIE shows highly increased currents (about 2.4 times) compared to the initial hydrogenated planar BDD electrode.[77] The enlarged redox currents of boron-doped diamond nanopillars obtained by masked or maskless RIE might result from the generation of surface defects by RIE. Hydrogenation of the boron-doped diamond nanopillars can also enhance the redox current. In addition, the electrochemical properties of the etched diamond nanopillars are heavily dependent on the length of the nanopillars. Szunerits and co-workers reported maskless-etched long and short boron-doped diamond nanopillars for the direct electrochemical detection of glucose under strong basic (pH 12) conditions. The electrochemical behavior of the short and long BDD NWs was investigated by cyclic voltammetry. Hydrogen-terminated electrodes show reversible redox behavior with currents being about 2.4 times larger with short BDD nanopillars and 3.5 times larger with long BDD nanopillars compared to that recorded on the flat BDD.[76,77]

Besides boron-doped diamond nanopillars obtained by RIE, N_2-incorporated ultra-nanocrystalline diamond nanowires (UNCDNWs) obtained by the microwave plasma CVD process also possess good electrochemical properties.[112,113] The electrochemical properties of the N_2-incorporated UNCDNWs are heavily dependent on the concentration of the incorporated N_2 in the Ar/CH_4 plasma. The lower conductivities of $UNCDNW_{3.4}$ and $UNCDNW_{5.0}$ (3.4% and 5% N_2 in Ar/CH_4 plasma, respectively) result in them showing smaller redox currents than the boron-doped planar BDD electrode. In contrast, the conductive $UNCDNW_{10}$, $UNCDNW_{20}$, and $UNCDNW_{25}$ films show larger redox currents and smaller separation between the anodic and cathodic peaks ($\Delta E_p = 73$–79 mV) than the boron-doped planar BDD electrode, thus showing their better electrochemical properties. The separation between the anodic and cathodic peaks (ΔE_p) indicates a degree of reversibility of the electrochemical reaction. The ΔE_p value of $UNCDNW_{10}$ is even lower than that of the RIE-etched boron-doped diamond nanopillars ($\Delta E_p = 868$ mV),[113] thus showing that the electrochemical reaction on $UNCDNW_{10}$ is more reversible than that on the RIE-etched boron-doped diamond nanopillars. However, a smaller separation between the anodic and cathodic peaks (ΔE_p) can be achieved by increasing the concentration of boron doping in the etched diamond nanopillars to $> 3 \times 10^{20}$ cm^{-3}.[70] Moreover, boron-doped diamond nanowire arrays obtained from the CVD method with a Si nanowire template also possess better electrochemical properties than planar BDD electrode, including larger redox currents and smaller ΔE_p values.

Furthermore, diamond shows the strongest bonding stability to deoxyribonucleic acid (DNA).[48] Applications of diamond electrodes in electrochemistry[49–51] and in biosensors[52–54] have been well-demonstrated. The electronic and chemical properties can be tuned by changing the surface termination of the diamond.[160] BDD electrodes have been consequently used for a wide range of electrochemical applications.[49,158] In the past few years, the surface area of diamond nanowires has been increased to achieve higher sensitivity and selectivity than planar BDD interfaces.[68,69] For example, experimental results show that the good biocompatibility and electron-transportation ability of a nanograss array BDD greatly improve the direct electron transfer and can make it suitable for the anode of high-performance MFCs.[161] The nanograss array BDD showed higher electrocatalytic activity toward catechol detection than did the as-grown BDD planar electrodes.[162] The BDD nanograss array can enhance the chemiluminescence signals from the $[Ru(bpy)_3]^{2+}$/TPA system, as a result of the superior properties of the BDD nanograss array, such as improved electrocatalytic activity and accelerated electron transfer.[163] In addition, nanotextured diamond nanowire surfaces are promising for application as novel platforms for the direct electrochemistry of redox proteins and for the construction of novel biosensors.[164]

4. Application of Diamond Nanowires

4.1. Field Emission from Diamond Nanowires

Diamond is a good candidate for solid-state electron emitters because of its negative or very low electron affinity.[165] Electron emitters can be used in vacuum microelectronics such as Spindt-type emitters. Diamond has a negative electron affinity (NEA) when the diamond [111] surface is terminated by hydrogen atoms.[165,166] Nishimura et al. reported that the diamond [100] surface also exhibits the NEA property.[167] NEA permits diamond to be a superior field emitter.[168] Defects at the diamond tip may further assist the emission by providing a focal point for both the field and current.[169] There are many reports concerning field emission from chemical vapor deposited (CVD) diamond nanocrystals or diamond-like carbon thin films. To date, only a few examples of the synthesis and field emission study of 1D nanowire diamond based systems have been reported.

4.1.1. Electron Field Emission (EFE) from Planar Films of Diamond Nanowire Arrays

Diamond was expected to be the most promising cold cathode material with a low EFE threshold field because of the NEA of hydrogenated diamond surfaces.[170,171] It was demonstrated that the EFE of diamond could be strongly enhanced by structuring nanodiamond surfaces into nanopillar arrays by plasma etching.[172] Li and Hatta reported the electron field emission of highly aligned diamond nanopillars with diameters of 50 nm and heights of 500 nm that were obtained by RIE in O_2 plasma by using Fe as metal masks.[59] A field emission current over 1 μA at 130 V μm^{-1} was obtained from the diamond nanopillars, with a threshold field of about 44 V μm^{-1}. The authors also found that the metal mask played an important role in the electron field emission of the diamond nanopillars obtained from RIE in O_2 plasma with a metal mask.[60] The electron field emission property of Al-masked diamond nanopillars is clearly better

than that of Fe-masked diamond nanopillars. A field emission current over 10 μA at 100 V μm^{-1} from the Al-masked diamond nanopillars was obtained, which is 10 times higher than that of Fe-masked diamond nanopillars. The threshold field also decreased from 44 V μm^{-1} to about 30 V μm^{-1}, thus showing that the electron field emission property of the Al-masked diamond nanopillars is better than that of the Fe-masked ones. Of the Fe-, Al-, and Mo-masked diamond nanopillars studied, the authors also found that the Mo-masked ones possessed the best electron field emission properties. A field emission current over 10 μA at 80 V μm^{-1} was obtained with the Al-masked diamond nanopillars.[60] The CVD diamond nanowire films possess better electron field emission properties than the etched diamond nanopillars. Madaleno et al. reported the electron field emission of a diamond nanowire film obtained by the MPCVD method templated by SiO_2 nanowires in 1% CH_4, 98% Ar, and 1% H_2 at 120 Torr pressure.[95] The EFE was measured using a parallel plate diode structure (Figure 20A). Emission starts

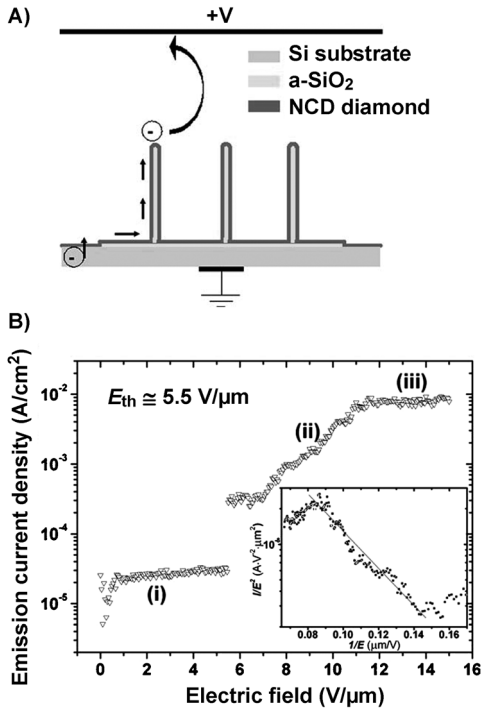

Figure 20. A) Schematic diagram representing electron flow from the Si substrate to emission at the fiber tip. B) Plot of the emission current density versus the external electric field of the as-synthesized NCD microtip array. Inset: corresponding FN plot. Reproduced from Ref. [95]. Copyright 2008, American Physical Society.

abruptly when the applied field reaches 5.5 V μm^{-1} (Figure 20B). This type of phenomenon was also reported by Jiang et al.[173] and Gupta et al.[174] with NCD films. A small plateau can be observed in the current density between 5.5 and 7 V μm^{-1}, after which the emission does not increase even if the applied field is increased. A similar behavior was reported by Gan et al.[175] in the electron emission from hydrogenated natural diamond. Electron field emission of nanodiamond nanowire arrays templated with SiO_2 nanowires was observed with a threshold field of 5.5 V μm^{-1}. A high emission current density of 10 mA cm^{-2} at 11 V μm^{-1} has been obtained, which is about 1000–10000 times larger than that of the etched diamond nanopilars (Fe-, Al-, and Mo-masked diamond nanopillars). The field-enhancement factor β can be taken from the slope of the FN plot, if we assume a work function of 4.6 eV, which is typical for graphitic materials. The experimental field-enhancement factor is $\beta = 2000$, which is extremely high. The authors then found that the electron field emission of nanodiamond nanowire arrays templated by SiO_2 nanowires was much improved when 20% N_2 was introduced into the gas source during the synthesis process.[94] The enhancement of the electron field emission properties of N_2-doped diamond nanowires is reflected in the lowering of the threshold field and in the increase of the current density. The threshold field decreases from 7.6 V μm^{-1} (diamond nanowires templated with SiO_2 nanowires and grown without N_2) to 3.5 V μm^{-1} (diamond nanowires templated by SiO_2 nanowires and grown in N_2), and the current density at 10 V μm^{-1} increases around 20 times with N_2 doping.

Very recently, Sankaran et al. reported the synthesis of conducting diamond nanowire (DNW) films by microwave plasma enhanced chemical vapor deposition with N_2.[176] The EFE properties of the DNWs encased by the highly conducting graphite were tested. The results show the emission current density J to be a function of the applied electric field E. A low turn-on field of 4.35 V μm^{-1} at a current density of 3 μA cm^{-2} was found. In addition, the current density increases rapidly and reaches the large value of about 3.42 mA cm^{-2} at a field of 9.1 V μm^{-1}. The DNW film exhibits far more efficient EFE properties with lower E_0 and highest J_e values than that of other diamond-related materials reported previously.[177–179] This excellent EFE feature of DNW films suggest great potential for flat panel display applications.[180] In conclusion, both etched diamond nanopillars and CVD-grown diamond nanowires show good field emission properties. Compared to etched diamond nanopillars, all the CVD-grown diamond nanowires, including diamond nanowires templated by SiO_2 nanowires and N_2-incorporated MPCVD diamond nanowires, possess better field emission properties, with a low-threshold and high current density. The ultrathin diamond nanorods produced by the microwave plasma assisted chemical vapor deposition method in the presence of a gas mixture of nitrogen and methane shows the best field emission properties of all the diamond nanowires.

4.1.2. *Electron Field Emission from a Single Diamond Nanowire*

Hsu and Xu reported the first measurement of the field emission from a single diamond nanowire from samples synthesized by a catalyst-assisted chemical vapor deposition method at atmospheric pressure.[40] Figure 21 shows the results as an I–V plot with a near-linear Fowler–Nordheim (F-N) relationship and an electron field emission with an ultralow threshold. By taking $\phi = 5$ eV for diamond, as suggested by Shiraishi and Ata,[43] it was found that the field-enhancement factor β reached about 60000. This is

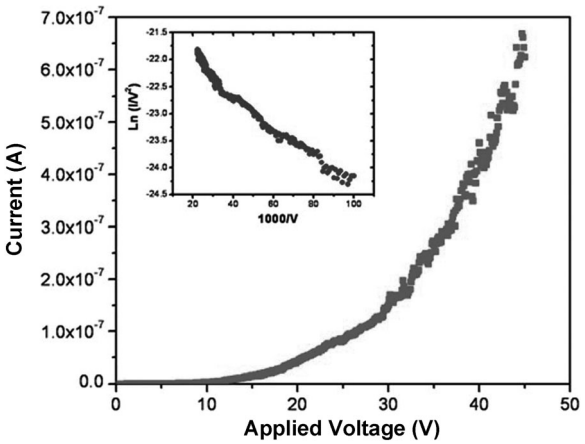

Figure 21. Field emission data obtained from an individual diamond nanowire in an SEM by a nanomanipulator. The inset shows the emission current data plotted in Fowler–Nordheim coordinates, thereby demonstrating the field emission behavior of the diamond nanowire. Reproduced from Ref. [40]. Copyright 2012, Royal Society of Chemical.

almost two orders of magnitude larger than the factor reported for carbon nanotube field emitters (ca. 1000).[44] It is also worth noting the low threshold field (ETH). The threshold field is defined as the applied field required for an emission of a certain current, which was set to be 100 nA. The authors then compared their diamond nanowire to the field emission characteristic obtained from a single 80 nm diameter carbon nanotube reported by Smith and Silva.[45] The threshold field of the diamond nanowire is 1.25 $V\,\mu m^{-1}$, which is four times lower than that of the carbon nanotube at 5 $V\,\mu m^{-1}$. The possible reasons for such a remarkably high field-enhancement factor (60 times higher) and low threshold field (four times lower) of the diamond nanowire over carbon nanotubes are the negative electron affinity, the greatly intensified field at the tip of a large curvature, and the possible defects at the nanowire tip, which itself is a "geometric singularity".[46] Furthermore, the chemical inertness, high mechanical strength, and high thermal conductivity of the diamond nanowires allow them to endure a longer and more intense emission. In addition, the wide band gap and the chemical inertness make diamond nanowires suitable for applications in high-temperature and aggressive environments such as space or military applications.

4.2. Diamond Nanowires for Highly Sensitive Matrix-Free Mass Spectrometric Analysis of Small Molecules

Diamond-like carbon (DLC), an amorphous carbon with mixed levels of sp^3- and sp^2-hybridized carbon atoms, has been successfully used for matrix-free laser desorption/ionization mass spectrometry (LDI-MS), particularly for the analysis of small metabolites such as carbohydrates, lipids, and low-molecular-weight peptides.[181] More recently, Coffinier et al. reported, for the first time, the use of boron-doped diamond nanowires (BDD NWs) as an inorganic substrate for matrix-free LDI-MS analysis of small molecules.[78] The

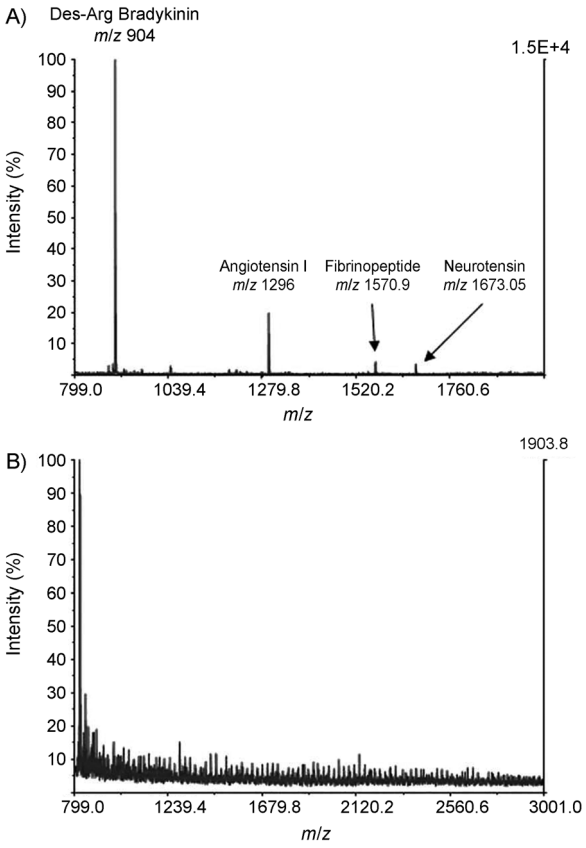

Figure 22. MS spectra obtained for a peptide mixture (50 $fmol\,\mu L^{-1}$) on A) BDD NWs and B) NcBDD starting material substrates. Reproduced from Ref. [78]. Copyright 2012, Royal Society of Chemical.

diamond nanowires were prepared by reactive-ion etching (RIE) of highly boron-doped (the boron level is 10^{19} $B\,cm^{-3}$) or undoped nanocrystalline diamond substrates with oxygen plasma. The resulting diamond nanowires were then coated with a thin silicon oxide layer that confers a superhydrophilic character to the surface. To minimize droplet spreading, the nanowires were chemically functionalized with octadecyltrichlorosilane (OTS) and then treated with UV/ozone to reach a final water contact angle of 120°. Figure 22 A shows the mass spectrum of the peptide mixture obtained at the BDD NW interface. As can be seen, all the peptides were detected with a relatively high signal intensity. As a control, the same experiment was performed on a planar nanocrystalline BDD, that is, the same interface without any RIE etching process. The absence of signals in the MS spectrum (Figure 22 B) clearly indicates that the presence of nanostructures on the BDD substrate is mandatory for the detection and identification of biomolecules. The signal to noise (S/N) ratios obtained with BDD nanowires were 1078:1, 431:1, 55:1, and 59.3:1 for [Des-Arg1]-bradykinin, angiotensin I, [Glu1]-fibrinopeptide B, and neurotensin, respectively, whereas those obtained on UDD nanowires were 115:1, 44:1, 8.3:1, and 4.3:1. We can notice that the S/N ratio values obtained using the UDD NWs are very low compared with those with BDD NWs, which suggests that to obtain an efficient detection and identification on diamond, the surface should be nanostruc-

tured with a dense layer of wires and display antireflective properties. Boron-doped diamond nanowire substrates were successfully used as energy-absorbing materials under UV laser irradiation, which allowed the detection and identification of small molecules by mass spectrometry.

4.3. Suspended Single-Crystal Diamond (SCD) Nanowires for High-Performance Nano-Electromechanical Switches

The current nano- or micro-electromechanical systems (N/MEM) based on silicon technologies suffer from problems of stiction, abrasion, and poor mechanical and tribological properties, which leads to the poor reliability of the electric contacts.[160,182] In particular, silicon-based switches are not able to work under extreme conditions such as high temperature, environments with corrosive chemicals, high-speed/high-power radio-frequency switches, etc. Diamond is the ideal material for high-performance N/MEM devices because of its outstanding properties such as its extremely high Young's modulus, its highest hardness, hydrophobic surface, low mass density, its highest thermal conductivity, high corrosion resistance to caustic chemicals, and biocompatibility. However, all the reported diamond N/MEM devices are based on polycrystalline or nanocrystalline films, which have the disadvantages of the existence of grain boundaries, impurities, and large stresses in the films; difficulty in controlling the electrical conductivity; and poor reproducibility.[183,184] Therefore, N/MEM devices made from these diamonds suffer from degradation in performance and poor reproducibility.

Liao et al. demonstrated high-performance all-SCD nano-electromechanical (NEM) systems by developing a batch fabrication process for suspended SCD nanowires with well-controlled dimensions and by proposing a lateral device concept.[47] The single-crystal diamond (SCD) NEM switches utilize a unique concept of diamond (conductor)-on-diamond (insulator), different from those of silicon-based techniques. It has been shown that the SCD NEM switches exhibit no stiction, high controllability, high reproducibility, high-temperature stability above 500 K, and repeated switching. This study not only opens a novel class of NEM switches based on the concept of diamond-on-diamond, but also has an extensive impact on the field of NEM systems. The NEM switching devices exhibit extremely low leakage currents (< 0.1 pA), which provides a high ON/OFF ratio of more than 6 orders of magnitude. The power consumption of this device in the OFF state is lower than 1 pW, which was calculated from the gate voltage and source leakage current. A high Young's modulus of the SCD nanowires provides a high lateral resonant frequency for high-speed switching. For example, the lateral fundamental resonant frequency for a cantilever with a width of 400 nm and a length of 5 μm reaches around 50 MHz, which corresponds to a maximum switching speed of 20 ns. The speed could be as fast as 3 ns if the cantilever length was reduced to 2 μm. With the steady development of SCD wafer technology, accompanied by cost reduction, the diamond NEM switch may rival Si-NEM structures. In particular, the resulting switches also function under harsh environments as a result of their all-SCD nature. On the other hand, since no p–n junction is required for NEM switches, the challenge of shallow doping a semiconductor diamond, which has been an issue for decades, can be circumvented by using the electromechanical switching approach.[185,186]

4.4. Diamond Nanowires for Scanning Probe Microscopy (SPM) Probes

SPM techniques such as atomic force microscopy (AFM), scanning tunneling microscopy (STM), scanning spreading resistance microscopy (SSRM), and scanning electrochemical microscopy (SECM) provide direct and reliable access to the structure of materials on the nanoscale, which is nowadays indispensable for almost all scientific fields. Diamond has been recognized as a perfect material for fabricating SPM probes because of its unrivalled physical and chemical properties. The CVD diamond thin film technology has resulted in diamond-coated Si tips now being widely commercially available and showing improved performance.[187,188] Furthermore, all-pyramidal diamond tips constructed by molding techniques have also attracted much interest.[189,190]

Recently, diamond nanowires were grown to be used as AFM tips by plasma etching of diamond films which were coated on standard Si AFM tips.[62] The idea was derived from the finding that enhanced resolution could be achieved by mounting[191] or growth[192] of sharp objects such as carbon nanotubes on commercial AFM tips. To grow diamond nanowires, firstly, NCD layers are deposited on standard Si AFM tips. The resulted tips are then treated in an O_2 ICP plasma for 30 s with an Au mask formed by thermally annealing a thin Au layer. The sharp diamond nanowires with apex radii at the tips of 5 nm are obtained after etching treatments. The fabricated scanning tips showed improved resolution and low tip wear relative to the standard Si tips and commercial diamond-coated tips when imaging nanocrystalline diamond surface and DNA.[62]

4.5. Diamond Nanowires for Photonic Systems

The development of material-processing techniques that can be used to generate optical diamond nanostructures containing a single-color center is an important problem in quantum science and technology. Light-emitting defects (color centers) in diamond are increasingly attractive for incorporation in a solid-state platform. For example, color centers based on nitrogen,[7,8] silicon,[10] carbon,[11] nickel,[12] and chromium[13] impurities have been shown to generate nonclassical states of light and emit single photons at room temperature, which is a critical resource for quantum optical communication systems. Hausmann et al. presented two scenarios for the combination of ion implantation and top-down diamond nanofabrication: diamond nanopillars and diamond nanowires.[42] The first approach consists of a "shallow" implant (20 nm) to generate nitrogen-vacancy (NV) color centers near the top surface of the diamond crystal prior to device fabrication. Individual NV centers are then

mechanically isolated by etching a regular array of nanopillars in the diamond surface. Photon antibunching measurements indicate that a high yield (>10%) of the devices contain a single NV center. In the second type of devices, the authors modify the approach slightly and implant single NV centers in diamond nanowire antennas. Nanowire arrays with diameters of about 200 nm and heights of 2 μm were fabricated in a single diamond chip by an RIE etching process. ^{15}N was then implanted in the diamond nanowires at 1.7 MeV and a dosage of 1×10^{9} cm^{-2}, and then annealed at 750 °C in a high vacuum ($<10^{-6}$ Torr) for 2 h. The calculation results indicated that this produces a layer of NV centers about 1.0 μm below the diamond surface. The reduced dosage, used to potentially minimize implantation-related damage (important for future low-temperature studies), resulted in a relatively low yield of nanowires containing a single NV center. Photon antibunching in the nanowire fluorescence $g^{(2)}(0)\approx0.06$ was possible without background subtraction, which represents a fivefold reduction compared to nanowire devices with type Ib material.[7] In addition, photon antibunching $g^{(2)}(0)<0.5$ is sustained at pump powers where the single-photon signal is saturated. The high single-photon flux of the nanowire geometry, combined with the low background fluorescence of the ultrapure diamond, allowed sustained photon antibunching to be observed even at high pump powers. Burek et al. reported a three-dimensional fabrication technique based on anisotropic plasma etching at an oblique angle to the sample surface. As a proof of concept, this angled-etching method was used to fabricate free-standing nanoscale components in bulk single-crystal diamond, including nanobeam mechanical resonators, optical waveguides, and photonic crystal and microdisk cavities. With the ability to create suspended nanobeam structures at virtually arbitrary angles and curvatures, the angled-etching process is a novel platform for realizing integrated photonic and mechanical structures in bulk media. This nanofabrication method will have an impact on a wide variety of areas, ranging from classical and quantum photonic devices to NEM-based sensors and actuators.[193–195]

4.6. Diamond Nanowires for Electrochemical Sensors

BDD electrodes have been used for a wide range of electrochemical applications.[49,158] In the past few years, studies on diamond nanowires were focused on increasing the surface area of the electrode to achieve higher sensitivity and selectivity compared to planar BDD interfaces.[1,196–198]

4.6.1. Diamond Nanowires for DNA Sensing

Yang et al. introduced for the first time the electrochemical application of vertically aligned diamond nanowires for DNA sensing. Nanowires separated by approximately 11 nm were selected because anchoring DNA molecules onto these wires would result in a DNA density of about 10^{12} cm^{-2}, which is promising for DNA sensing with high efficiency.[31,69,70] The tips of the nanowires are functionalized electrochemically with phenyl groups. Such functionalized nanowires are used to bond geometrically controlled oligonucleotide molecules to diamond. As the DNA self-aligns with the phenyl linker groups, functionalization of the nanowire tips produces a pattern of dispersed DNA bonding that is governed by the structure of the nanowires. Sensitivity curves for DNA hybridization were measured by varying the concentration of complementary target DNA from 1 μM to 10 pM. Sensing with diamond nanowires is about 100 to 1000 times better than with smooth surfaces of Au or polycrystalline diamond. To identify the sensitivity limit exactly, experiments with between 0 and 10 pm of complementary DNA were performed, and the results indicate a sensitivity limit of around 2 pm. No degradation of the DNA on the nanowires was detected over 30 cycles of DNA hybridization/denaturation, which is comparable with the chemical stability of optical DNA biosensors based on diamond.[48]

4.6.2. Diamond Nanowires for Amperometric Glucose Biosensing

Szunerits and co-workers reported maskless etched boron-doped diamond nanopillars for the direct electrochemical detection of glucose under strong basic (pH 12) conditions. A linear relationship between the current and glucose concentration in the range of 60 μM to 8 mM was obtained with a correlation coefficient of $r^2=0.999$ according to $i(\mu A)=-0.50+49.34[\text{glucose}]$. The detection limit of glucose was determined to be 60 μM from five blank noise signals (95% confidence level).[76] The results reported by Nebel and co-workers showed that the Ni-coated etched diamond nanopillar electrode can greatly improve the sensitivity of the sensor for glucose detection.[35] Ni-coated diamond nanopillars were fabricated through a Ni-masked RIE process. Planar boron-doped diamond (BDD) films were first grown in an ellipsoidal-shaped microwave plasma enhanced chemical vapor deposition system. Briefly, after growth of the planar BDD, a thin Ni layer (2–5 nm) was evaporated on to it. Annealing this layer in a vacuum at 700 °C for 5 min resulted in the homogeneous formation of Ni nanoparticles on the diamond surface. These Ni nanoparticles were then used as the etching mask for the RIE etching process in an O_2 plasma. As Ni is resistive in oxygen atmospheres, diamond nanopillars were obtained, whose tips were coated with Ni nanoparticles. The redox current on Ni-coated diamond nanopillars is 30 times higher than that on planar BDD electrodes, and 6 times higher than that on bare nanopillars. The enhancement of the current on Ni-coated diamond nanopillars is proportional to the concentration of glucose in the range of 10 μM to 1 mM, and the detection limit of glucose was determined to be 10 μM, which is about 6 times more sensitive than the results of Szunerits et al.

Diamond nanowire electrodes obtained from the CVD method show more sensitivity than the etched diamond nanopillars to glucose. Our research group reported the synthesis of films of boron-doped diamond nanowire arrays by the hot-filament chemical vapor deposition (HFCVD) method using Si nanowires as a template.[96] This BDDNW electrode exhibits a very attractive electrochemical performance compared to conventional planar boron-doped dia-

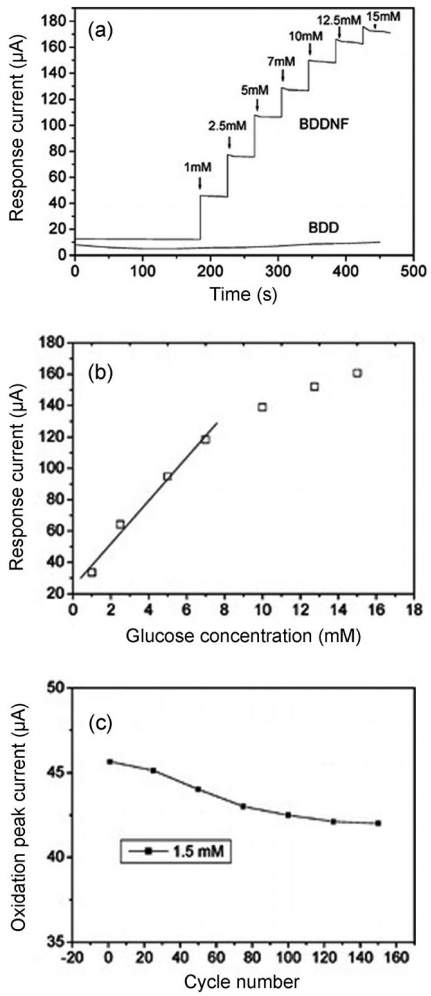

Figure 23. a) Current–time responses of the BDDNF and BDD electrodes to a stirred solution containing 0.1 M NaOH at an applied potential of 0.7 V (versus SCE). b) Calibration curve of the BDDNF electrode at a working potential of 0.7 V (versus SCE). c) Long-term electrochemical cycling stability of the BDDNF electrode for 1.5 mM glucose. Reproduced from Ref. [96]. Copyright 2009, American Chemical Society.

mond (BDD) electrodes, with notably improved sensitivity and selectivity for biomolecule detection. As shown in Figure 23a, it is clear that the electrochemical response to glucose at the BDDNF electrode is very fast at reaching a dynamic equilibrium upon each addition of the sample solution, thereby generating a steady-state current signal within a short time (less than 20 s). The calibration curve for the electrochemical response of the BDDNF electrode to glucose at 0.7 V (versus SCE) is shown in Figure 23b. The response to glucose is linear over a range from 0 to 7 mM, with a correlation coefficient (R) of 0.993 and a sensitivity of 8.1 $\mu A\,mM^{-1}\,cm^{-2}$ (slope). The limit of detection was estimated at a signal-to-noise ratio of 3:1 to be $0.2+0.01$ μM, which is 300 times more sensitive than bare diamond nanopillars, and is 50 times more sensitive than Ni-coated diamond nanopillars. The loss of the electrochemical activity was about 8% after 150 repetitive cycles, which suggests that the BDDNW electrode is relatively stable because of the inertness of the H-terminated diamond surface (Figure 23c). Moreover, the BDDNF electrode is very favorable for the selective determination of glucose in the presence of ascorbic acid (AA) and uric acid (UA).

4.6.3. Diamond Nanowires for Tryptophan Sensing

Szunerits et al. reported on the fabrication and electrochemical investigation of boron-doped diamond nanopillar electrodes.[77] The nanopillars were obtained directly from highly doped polycrystalline diamond substrates by reactive-ion etching (RIE) with oxygen plasma. The interface with the most favorable electrochemical response was investigated for the detection of tryptophan by differential pulse voltammetry. The direct detection of tryptophan by differential pulse voltammetry (DVP) was previously reported for polycrystalline BDD by Zhao et al.[199] A linear relationship between the oxidative peak at $E \approx 1.02$ V versus SCE and the concentration of tryptophan was observed, with a detection limit of 1×10^{-5} M. In this study, the authors used similar conditions for the electrochemical detection of tryptophan at oxidized BDD NW interfaces. As shown in Figure 24, a detection limit of $5\times$

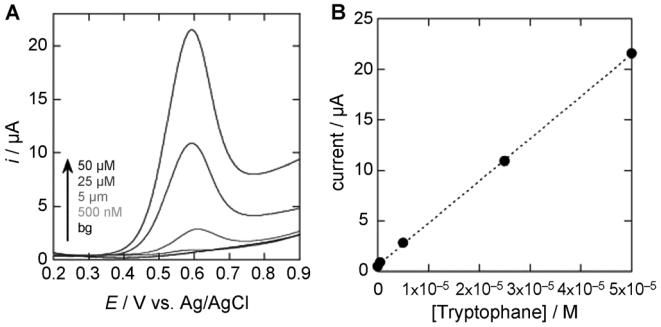

Figure 24. A) Differential pulse voltammograms of different concentrations of tryptophan (50 μM, 25 μM, 5 μM, 0.5 μM) in Na_2PO_4/NaOH (pH 11) on oxidized BDD NWs; bg = background. B) Calibration curve. Reproduced from Ref. [77]. Copyright 2010, Elsevier.

10^{-7} M was obtained on BDD NWs. This is significantly lower than on planar polycrystalline BDD,[199] but an order of magnitude higher than reported on glassy carbon electrodes modified with single-walled carbon nanotube films.[200] Very recently, Szunerits and co-workers reported the simultaneous detection of tryptophan and tyrosine by electrochemical means using etched diamond nanopillars when the proportion of tryptophan present in the mixtures of Tryp and Tyr was not larger than Tryp/Tyr $\leq$ 0.5:1. For the planar BDD electrode, the detection limit was 5 μM for tryptophan and tyrosine in individual solutions, 10 μM for tryptophan (in the presence of 500 μM tyrosine), and 20 μM for tyrosine (in the presence of 50 μM tryptophan) from five blank noise signals (95% confidence level), while lower detection limits of about 0.5 μM and 0.2 μM were obtained for tryptophan and tyrosine with BDD nanopillars.[201]

4.6.4. Diamond Nanowires for Dopamine Sensing

Shalini et al. reported the in situ detection of dopamine using a nitrogen-incorporated diamond nanowire electrode.[113] DNW films were grown on planar Si substrates using a microwave plasma enhanced chemical vapor deposition (MPECVD) method. The N_2-rich plasma led to an increase in the sp^2-hybridized graphitic phase. The nanowire-like structure could be responsible for the outstanding electrochemical properties, and exhibits considerable potential for biosensing applications. The electrodes based on a DNW film with incorporated N_2 show excellent electrocatalytic activity towards the oxidation of small molecules, such as ascorbic acid (AA), dopamine (DA), and uric acid (UA). The electrochemical behavior of conducting DNW films with incorporated N_2 has been studied by CV and DPV in both the absence and presence of AA and UA. The DPV results show that the DNW electrodes with incorporated N_2 exhibit high electrocatalytic activity for the oxidation of AA and UA. A high selectivity and reliable antifouling ability may result in the DNW film electrodes being an effective sensor for the direct determination of AA, DA, and UA in a real sample.

5. Conclusions and Outlook

Numerous studies have focused on developing the various synthetic methods to prepare diamond nanowires. However, the synthesis of these diamond nanowires has proven to be a low probability event and very difficult to reproduce. RIE, a conventional technique in the semiconductor industry, has shown great potential for fabricating nanoscale patterns because of its high anisotropic nature and fine controllability. Various gas mixtures and masks have been developed for etching diamond nanopillars. Despite the promising progress made in fabricating diamond nanopillars, challenges still remain when fabricating practical devices based on diamond nanopillars by RIE. Firstly, it is not easy to fully understand the basic mechanisms in RIE because the parameters are mutually affected by each other and a better understanding of the procedure of plasma etching is essential to make the processes and products more controllable. Secondly, as the material systems become multicomponent and multifunctional, it is harder and harder to preferentially remove specific materials, such as reaction gas and masks, without affecting others when trying to achieve precision at the as-etched diamond nanopillars. As a consequence of the chemical inertness of sp^3-hybridized carbon, although diamond nanowires are energetically favorable compared to carbon nanotubes, few diamond nanowire structures have been observed experimentally by the CVD method. CVD synthesis assisted by a nanowire template, including SiO_2 nanowire templates and Si nanowire templates, is an effective approach for realizing reproducible diamond nanowires because of its unparalleled ability to produce nanostructures in a highly controlled manner. However, is very difficult to remove the template materials which are encapsulated in the diamond nanowires. In addition, this method cannot realize the large-scale production of diamond nanowires. Although there are challenges, it can be expected that the combination of the top-down and bottom-up approaches may be a better solution for the realization of large-scale diamond nanowires.

On other hand, simulation and experiments have verified that 1D diamond nanowires possess excellent properties, including mechanical, electron field emission, structural stability, good electrochemical properties, and so on. Many practical applications, such as EFE devices, high-performance nano-electromechanical switches, and electrochemical biosensor etc., have been developed. However, the promise of diamond nanowires in applications has not been fulfilled. For example, despite the impressive progress in the development of BDD-based amperometric biosensors, the promise of the application of these biosensors in real biological systems has not been realised, and there are still many challenges and obstacles related to the achievement of the highly stable and reliable continuous monitoring of biomolecules.

Future developments in the applications will rely upon the large-scale synthesis of diamond nanowires, and the close collaboration of analytical technology, electrochemistry, biological engineering, nanoelectronics, and other related technologies. Continued investigation into this area will likely yield many new synthetic approaches and open up broader application areas for diamond nanowires.

We thank the support from the International Science & Technology Cooperation Program of China (no. 2013DFG50150), the Natural Foundation of Sciences of the People's Republic of China (Grant no. 211375137.

Received: December 13, 2013
Published online: November 5, 2014

[1] S. Szunerits, R. Boukherroub, *J. Solid State Electrochem.* **2008**, *12*, 1205 – 1218.
[2] M. Soileau, J. O. Porteus, D. L. Decker, *Applied Optics*, **1980**, *19*, 3043 – 3044.
[3] E. Fortin, J. Chane-Tune, P. Mailley, S. Szunerits, B. Marcus, J. P. Petit, M. Mermoux, E. Vieil, *Bioelectrochemistry* **2004**, *63*, 303 – 306.
[4] Y. V. Pelskov, A. Y. Sakharova, M. D. Krotova, *J. Electroanal. Chem.* **1987**, *228*, 19 – 27.
[5] A. Kapałka, G. Fóti, C. Comninellis, *Elecrochim. Acta* **2009**, *54*, 2018 – 2023.
[6] J. T. Choy, B. J. M. Hausmann, T. M. Babinec, I. Bulu, M. Khan, P. Maletinsky, A. Yacoby, M. Loncar, *Nat. Photonics* **2011**, *5*, 738 – 743.
[7] C. Kurtsiefer, S. Mayer, P. Zarda, H. Weinfurter, *Phys. Rev. Lett.* **2000**, *85*, 290 – 293.
[8] A. Beveratos, R. Brouri, T. Gacoin, J. P. Poizat, P. Grangier, *Phys. Rev. A* **2001**, *64*, 061802.
[9] T. M. Babinec, B. J. M. Hausmann, M. Khan, Y. Zhang, J. R. Maze, P. R. Hemmer, M. Loncar, *Nat. Nanotechnol.* **2010**, *5*, 195 – 199.
[10] C. Wang, C. Kurtsiefer, H. Weinfurter, B. Burchard, *J. Phys. B* **2006**, *39*, 37 – 41.
[11] B. Naydenov, R. Kolesov, A. Batalov, J. Meijer, S. Pezzagna, D. Rogalla, F. Jelezko, J. Wrachtrup, *Appl. Phys. Lett.* **2009**, *95*, 181109.
[12] T. Gaebel, I. Popa, A. Gruber, M. Domhan, F. Jelezko, J. Wrachtrup, *New J. Phys.* **2004**, *6*, 98.

[13] I. Aharonovich, S. Castelletto, D. A. Simpson, A. Stacey, J. McCallum, A. D. Greentree, S. Prawer, *Nano Lett.* **2009**, *9*, 3191 – 3195.
[14] F. Jelezko, T. Gaebel, I. Popa, A. Gruber, J. Wrachtrup, *Phys. Rev. Lett.* **2004**, *92*, 076401.
[15] L. Childress, J. M. Taylor, A. S. Sorensen, M. D. Lukin, *Phys. Rev. Lett.* **2006**, *96*, 070504.
[16] K. Enke, H. Dimigen, H. Hübsch, *Appl. Phys. Lett.* **1980**, *36*, 291.
[17] X. Jiang, C. L. Jia, *Appl. Phys. Lett.* **2002**, *80*, 2269 – 2271.
[18] Z. Yao, H. W. C. Postma, L. Balents, C. Dekker, *Nature* **1999**, *402*, 273 – 276.
[19] J. O. Orwa, S. Prawer, D. N. Jamieson, J. L. Peng, J. C. McCallum, K. W. Nugent, Y. J. Li, L. A. Bursill, S. P. Withrow, *J. Appl. Phys.* **2001**, *90*, 3007.
[20] T. Irifune, A. Kurio, S. Sakamoto, T. Inoue, H. Sumiya, *Nature* **2003**, *421*, 599 – 600.
[21] V. Brazhkin, N. Dubrovinskaia, A. Nicol, N. Novikov, R. Riedel, R. Solozhenko, Y. Zhao, *Nat. Mater.* **2004**, *3*, 576 – 577.
[22] G. Zheng, F. Patolsky, Y. Cui, W. U. Wang, C. M. Lieber, *Nat. Biotechnol.* **2005**, *23*, 1294 – 1301.
[23] Y. Cui, Q. Wei, H. Park, C. M. Lieber, *Science* **2001**, *293*, 1289 – 1292.
[24] O. A. Shenderova, D. W. Brenner, R. S. Ruoff, *Nano Lett.* **2003**, *3*, 805 – 809.
[25] A. S. Barnard, S. P. Russo, I. K. Snook, *Nano Lett.* **2003**, *3*, 1323 – 1328.
[26] A. S. Barnard, S. P. Russo, I. K. Snook, *Philos. Mag.* **2004**, *84*, 899 – 907.
[27] A. S. Barnard, I. K. Snook, *J. Chem. Phys.* **2004**, *120*, 3817 – 3821.
[28] H. Shiomi, *Jpn. J. Appl. Phys.* **1997**, *36*, 7745 – 7748.
[29] H. Masuda, M. Watanabe, K. Yasui, D. Tryk, T. Rao, A. Fujishima, *Adv. Mater.* **2000**, *12*, 444 – 447.
[30] C. Terashima, K. Arihara, S. Okazaki, T. Shichi, D. A. Tryk, T. Shirafuji, N. Saito, O. Takai, A. Fujishima, *ACS Appl. Mater. Interfaces* **2011**, *3*, 177 – 182.
[31] N. Yang, H. Uetsuka, E. Osawa, C. E. Nebel, *Angew. Chem.* **2008**, *120*, 5261 – 5263; *Angew. Chem. Int. Ed.* **2008**, *47*, 5183 – 5185.
[32] Y. Ando, Y. Nishibayashi, K. Kobashi, T. Hirao, K. Oura, *Diamond Relat. Mater.* **2002**, *11*, 824 – 827.
[33] E. S. Baik, Y. J. Baik, S. W. Lee, D. Jeon, *Thin Solid Films* **2000**, *377 – 378*, 295 – 298.
[34] W. Smirnov, A. Kriele, N. Yang, C. E. Nebel, *Diamond Relat. Mater.* **2010**, *19*, 186 – 189.
[35] N. Yang, W. Smirnov, C. E. Nebel, *Electrochem. Commun.* **2013**, *27*, 89 – 91.
[36] L. T. Sun, J. L. Gong, Z. Y. Zhu, D. Z. Zhu, Z. X. Wang, W. Zhang, J. G. Hu, Q. T. Li, *Diamond Relat. Mater.* **2005**, *14*, 749 – 752.
[37] L. T. Sun, J. L. Gong, D. Z. Zhu, Z. Y. Zhu, S. X. He, *Adv. Mater.* **2004**, *16*, 1849 – 1853.
[38] N. Dubrovinskaia, L. Dubrovinsky, *Appl. Phys. Lett.* **2005**, *87*, 083106.
[39] C. H. Hsu, S. G. Cloutier, S. Palefsky, J. Xu, *Nano Lett.* **2010**, *10*, 3272 – 3276.
[40] C. H. Hsu, J. Xu, *Nanoscale* **2012**, *4*, 5293 – 5299.
[41] B. J. M. Hausmann, M. Khan, Y. Zhang, T. M. Babinec, K. Martinick, M. McCutcheon, P. R. Hemmer, M. Loncar, *Diamond Relat. Mater.* **2010**, *19*, 621 – 629.
[42] B. J. M. Hausmann, T. M. Babinec, J. T. Choy, J. S. Hodges, S. Hong, I. Bulu, A. Yacoby, M. D. Lukin, M. Loncar, *New J. Phys.* **2011**, *13*, 045004.
[43] M. Shiraishi, M. Ata, *Carbon* **2001**, *39*, 1913 – 1917.
[44] Z. Xu, X. D. Bai, E. G. Wang, Z. L. Wang, *Appl. Phys. Lett.* **2005**, *87*, 163106.
[45] R. C. Smith, S. R. P. Silva, *J. Appl. Phys.* **2009**, *106*, 014314.
[46] A. Mayer, N. M. Miskovsky, P. H. Cutler, *Phys. Rev. B* **2002**, *65*, 195416.
[47] M. Y. Liao, S. Hishita, E. Watanabe, S. Koizumi, Y. Koide, *Adv. Mater.* **2010**, *22*, 5393 – 5397.
[48] W. Yang, O. Auciello, J. E. Butler, W. Cai, J. A. Carlisle, J. E. Gerbi, D. M. Gruen, T. Knickerbocker, T. L. Lasseter, J. N. Russell, J. Smith, R. J. Hamers, *Nat. Mater.* **2002**, *1*, 253 – 257.
[49] Y. Zhou, J. Zhi, Y. Zou, W. Zhang, S. T. Lee, *Anal. Chem.* **2008**, *80*, 4141 – 4146.
[50] T. Watanabe, T. A. Ivandini, Y. Makide, A. Fujishima, Y. Einaga, *Anal. Chem.* **2006**, *78*, 7857 – 7860.
[51] A. Suzuki, T. A. Ivandini, K. Yoshimi, A. Fujishima, G. Oyama, T. Nakazato, N. Hattori, S. Kitazawa, Y. Einaga, *Anal. Chem.* **2007**, *79*, 8608 – 8615.
[52] H. Gu, X. D. Su, K. P. Loh, *J. Phys. Chem. B* **2005**, *109*, 13611 – 13618.
[53] W. Yang, J. E. Butler, J. N. Russell, R. J. Hamers, *Langmuir* **2004**, *20*, 6778 – 6787.
[54] B. Rezek, D. Shin, C. E. Nebel, *Langmuir* **2007**, *23*, 7626 – 7633.
[55] G. S. Oehrlein, *Phys. Today* **1986**, *39*, 26 – 33.
[56] C. Y. Li, Y. Hatta, *Diamond Relat. Mater.* **2005**, *14*, 1780 – 1783.
[57] Y. Tzeng, J. Wei, J. T. Woo, W. Lanford, *Appl. Phys. Lett.* **1993**, *63*, 2216 – 2218.
[58] E. S. Baik, Y. J. Baik, D. Jeon, *J. Mater. Res.* **2000**, *15*, 923 – 926.
[59] C. Y. Li, A. Hatta, *J. New Mater. Electrochem. Syst.* **2007**, *10*, 221 – 224.
[60] C. Y. Li, A. Hatta, *Diamond Relat. Mater.* **2006**, *15*, 357 – 360.
[61] Y. S. Zou, T. Yang, W. J. Zhang, Y. M. Chong, B. He, I. Bello, S. T. Lee, *Appl. Phys. Lett.* **2008**, *92*, 053105.
[62] W. Smirnov, A. Kriele, R. Hoffmann, E. Sillero, J. Hees, O. A. Williams, N. Yang, C. Kranz, C. E. Nebel, *Anal. Chem.* **2011**, *83*, 4936 – 4941.
[63] W. Janssen, E. Gheeraert, *Diamond Relat. Mater.* **2011**, *20*, 389 – 394.
[64] S. Okuyama, S. I. Matsushita, A. Fujishima, *Chem. Lett.* **2000**, 534 – 535.
[65] S. Okuyama, S. I. Matsushita, A. Fujishima, *Langmuir* **2002**, *18*, 8282 – 8287.
[66] M. Yamaki, J. Higo, K. Nagayama, *Langmuir* **1995**, *11*, 2975 – 2798.
[67] C. D. Dushkin, P. A. Kralchevsky, V. N. Paunov, H. Yoshimura, K. Nagayama, *Langmuir* **1996**, *12*, 641 – 651.
[68] N. Yang, H. Uetsuka, E. Osawa, C. E. Nebel, *Nano Lett.* **2008**, *8*, 3572 – 3576.
[69] N. Yang, H. Uetsuka, C. E. Nebel, *Adv. Funct. Mater.* **2009**, *19*, 887 – 893.
[70] N. Yang, H. Uetsuka, O. A. Williams, E. Osawa, N. Tokuda, C. E. Nebel, *Phys. Status Solidi A* **2009**, *206*, 2048 – 2056.
[71] N. Tokuda, H. Umezawa, T. Saito, K. Yamabe, H. Okushi, S. Yamasaki, *Diamond Relat. Mater.* **2007**, *16*, 767 – 770.
[72] A. Krüger, F. Kataoka, M. Ozawa, T. Fujino, Y. Suzuki, A. E. Aleksenskii, A. Y. Vul, E. Ösawa, *Carbon* **2005**, *43*, 1722 – 1730.
[73] Enhanced diamond nucleation on monodispersed nanocrystalline diamond: O. A. Williams, O. Douheret, M. Daenen, K. Haenen, E. Osawa, M. Takahashi, *Chem. Phys. Lett.* **2007**, *445*, 255 – 258.
[74] O. A. Williams, M. Daenen, J. D'Haen, K. Haenen, J. Maes, V. V. Moshchalkov, M. Nesladek, D. M. Gruen, *Diamond Relat. Mater.* **2006**, *15*, 654 – 658.
[75] M. Wei, C. Terashima, M. Lv, A. Fujishima, Z. Gu, *Chem. Commun.* **2009**, 3624 – 3626.
[76] Q. Wang, P. Subramanian, M. Li, W. Yeap, K. Haenen, Y. Coffinier, R. Boukherroub, S. Szunerits, *Electrochem. Commun.* **2013**, *34*, 286 – 290.
[77] S. Szunerits, Y. Coffinier, E. Galopin, J. Brenner, R. Boukherroub, *Electrochem. Commun.* **2010**, *12*, 438 – 441.

[78] Y. Coffinier, S. Szunerits, H. Drobecq, M. Oleg, R. Boukherroub, *Nanoscale* **2012**, *4*, 231 – 238.
[79] L. Marcon, A. Addad, Y. Coffinier, R. Boukherroub, *Acta Biomater.* **2013**, *9*, 4585 – 4591.
[80] Y. Coffinier, E. Galopin, S. Szunerits, R. Boukherroub, *J. Mater. Chem.* **2010**, *20*, 10671 – 10675.
[81] P. S. Shah, T. Hanrath, K. P. Johnston, S. A. Korgel, *J. Phys. Chem. B* **2004**, *108*, 9574 – 9587.
[82] Y. Wu, P. Yang, *J. Am. Chem. Soc.* **2001**, *123*, 3165 – 3166.
[83] S. Kodambaka, J. Tersoff, M. C. Reuter, F. M. Ross, *Science* **2007**, *316*, 729 – 732.
[84] J. L. Lensch-Falk, E. R. Hemesath, D. E. Perea, L. J. Lauhon, *J. Mater. Chem.* **2009**, *19*, 849 – 857.
[85] Y. Xia, P. Yang, Y. Sun, Y. Wu, B. Mayers, B. Gates, Y. Yin, F. Kim, H. Yan, *Adv. Mater.* **2003**, *15*, 353 – 389.
[86] H. Ringsdorf, B. Schlarb, J. Verzmer, *Angew. Chem.* **1988**, *100*, 117 – 162; *Angew. Chem. Int. Ed. Engl.* **1988**, *27*, 113 – 158.
[87] C. N. R. Rao, A. Govindaraj, F. L. Deepak, N. A. Gunari, M. Nath, *Appl. Phys. Lett.* **2001**, *78*, 1853 – 1855.
[88] Y. Yin, Y. Lu, Y. Sun, Y. Xia, *Nano Lett.* **2002**, *2*, 427 – 430.
[89] P. W. May, *Endeavour* **1995**, *19*, 101 – 106.
[90] S. S. Lee, O. Takai, H. Itoh, *J. Mater. Sci.* **1997**, *32*, 2417 – 2422.
[91] G. Chollon, R. Naslain, C. Prentice, R. Shatwell, P. May, *J. Eur. Ceram. Soc.* **2005**, *25*, 1929 – 1942.
[92] V. Baranauskas, H. J. Ceragioli, A. C. Peterlevitz, A. F. Durrant, *Thin Solid Films* **2001**, *398*, 250 – 254.
[93] M. K. Singh, E. Titus, J. C. Madaleno, G. Cabral, J. Gracio, *Chem. Mater.* **2008**, *20*, 1725 – 1732.
[94] M. K. Singh, E. Titus, M. G. Willinger, J. C. Madaleno, J. Gracio, *Diamond Relat. Mater.* **2009**, *18*, 865 – 869.
[95] J. C. Madaleno, M. K. Singh, E. Titus, G. Cabral, J. Gracio, *Appl. Phys. Lett.* **2008**, *92*, 023113.
[96] D. Luo, L. Wu, J. Zhi, *ACS Nano* **2009**, *8*, 2121 – 2128.
[97] D. Luo, L. Wu, J. Zhi, *Chem. Commun.* **2010**, *46*, 6488 – 6490.
[98] K. Peng, Y. J. Yan, S. P. Gao, J. Zhu, *Adv. Mater.* **2002**, *14*, 1164 – 1167.
[99] C. G. Granqvist, A. Andersson, O. Hundri, *Appl. Phys. Lett.* **1979**, *35*, 268 – 270.
[100] C. A. Huber, T. E. Huber, M. Sadoqi, J. A. Lubin, S. Mannlis, C. B. Prater, *Science* **1994**, *263*, 800 – 802.
[101] H. Masuda, T. Yanagishita, K. Yasui, K. Nishio, I. Yagi, T. N. Rao, A. Fujishima, *Adv. Mater.* **2001**, *13*, 247 – 249.
[102] F. Keller, M. S. Hunter, D. L. Robinson, *J. Electrochem. Soc.* **1953**, *100*, 411 – 419.
[103] H. Masuda, K. Fukuda, *Science* **1995**, *268*, 1466 – 1468.
[104] I. I. Vlasov, O. I. Lebedev, V. G. Ralchenko, E. Goovaerts, G. Bertoni, G. V. Tendeloo, V. I. Konov, *Adv. Mater.* **2007**, *19*, 4058 – 4062.
[105] I. I. Vlasov, V. G. Ralchenko, E. Goovaerts, A. V. Saveliev, M. V. Kanzyuba, *Phys. Status Solidi A* **2006**, *203*, 3028 – 3035.
[106] R. Arenal, P. Bruno, D. J. Miller, M. Bleuel, J. Lal, D. M. Gruen, *Phys. Rev. B* **2007**, *75*, 195431.
[107] D. M. Gruen, *Annu. Rev. Mater. Sci.* **1999**, *29*, 211 – 259.
[108] J. A. Nuth, *Nature* **1987**, *329*, 589.
[109] P. Badziag, W. S. Veowoerd, W. P. Ellis, N. R. Greiner, *Nature* **1990**, *343*, 244 – 245.
[110] N. Shang, P. Papakonstantinou, P. Wang, A. Zakharov, U. Palnitkar, I. N. Lin, M. Chu, A. Stamboulis, *ACS Nano* **2009**, *3*, 1032 – 1038.
[111] A. R. Sobia, S. Adnan, A. Mukhtiar, A. A. Khurram, A. A. Turab, A. Awais, A. Naveed, Q. J. Faisal, H. Javaid, G. J. Yu, *Curr. Appl. Phys.* **2012**, *12*, 712 – 717.
[112] J. Shalini, Y. C. Lin, T. H. Chang, K. J. Sankaran, H. C. Chen, C. Y. Lee, N. H. Tai, *Electrochim. Acta* **2013**, *92*, 9 – 19.
[113] J. Shalini, K. J. Sankaran, C. L. Dong, C. Y. Lee, N. H. Tai, I. N. Lin, *Nanoscale* **2013**, *5*, 1159 – 1167.
[114] L. Y. Zeng, H. Y. Peng, W. B. Wang, Y. Q. Chen, D. Lei, W. Qi, J. Q. Liang, J. L. Zhao, X. G. Kong, H. Zhang, *J. Phys. Chem. C* **2008**, *112*, 1401 – 1406.
[115] L. Y. Zeng, H. Y. Peng, W. B. Wang, Y. Q. Chen, D. Lei, W. Qi, J. Q. Liang, J. L. Zhao, X. G. Kong, H. Zhang, *J. Phys. Chem. C* **2008**, *112*, 6160 – 6164.
[116] F. P. Bundy, H. T. Hall, H. M. Strong, R. H. Wentorf, *Nature* **1955**, *176*, 51 – 55.
[117] B. V. Derjaguin, DV. Fedoseev, V. M. Lukyanovich, V. A. Ryabov, A. V. Lavrentyev, *J. Cryst. Growth* **1968**, *2*, 380 – 384.
[118] W. R. L. Lambrecht, C. H. Lee, B. Segall, J. C. Angus, Z. D. Li, M. Sunkara, *Nature* **1993**, *364*, 607 – 610.
[119] A. Gross, *Appl. Phys. A* **1998**, *67*, 627 – 635.
[120] H. F. Berger, E. Grosslinger, K. D. Rendulic, *Surf. Sci.* **1992**, *261*, 313 – 320.
[121] J. H. Zhang, B. Q. Wei, J. Liang, Z. D. Gao, D. H. Wu, *Mater. Lett.* **1997**, *31*, 79 – 82.
[122] Y. Q. Hou, D. M. Zhuang, G. Zhang, M. S. Wu, J. J. Liu, *Appl. Surf. Sci.* **2002**, *185*, 303 – 308.
[123] Y. Q. Zhu, T. Sekine, T. Kobayashi, T. Takazawa, M. Terrones, H. Terrones, *Chem. Phys. Lett.* **1998**, *287*, 689 – 693.
[124] B. Q. Wei, J. Liang, Z. D. Gao, J. H. Zhang, Y. Q. Zhu, Y. B. Li, D. H. Wu, *J. Mater. Process. Technol.* **1997**, *63*, 573 – 578.
[125] L. M. Cao, C. X. Gao, H. P. Sun, G. T. Zou, Z. Zhang, X. Y. Zhang, M. He, M. Zhang, Y. C. Li, J. Zhang, D. Y. Dai, L. L. Sun, W. K. Wang, *Carbon* **2001**, *39*, 311 – 314.
[126] H. Yusa, *Diamond Relat. Mater.* **2002**, *11*, 87 – 91.
[127] B. Wei, J. Zhang, J. Liang, D. Wu, *Carbon* **1998**, *36*, 997 – 1001.
[128] L. T. Sun, J. L. Gong, Z. Y. Zhu, D. Z. Zhu, S. X. He, *Appl. Phys. Lett.* **2004**, *84*, 2901 – 2903.
[129] J. Singh, *J. Mater. Sci.* **1994**, *29*, 2761 – 2766.
[130] N. Dubrovinskaia, L. Dubrovinsky, F. Langenhorst, S. Jacobsen, C. Liebske, *Diamond Relat. Mater.* **2005**, *14*, 16 – 22.
[131] J. Voskuhl, M. Waller, S. Bandaru, B. A. Tkachenko, C. Fregonese, B. Wibbeling, P. R. Schreiner, B. J. Ravoo, *Org. Biomol. Chem.* **2012**, *10*, 4524 – 4530.
[132] J. Zhang, Y. Feng, H. Ishiwata, Y. Miyata, R. Kitaura, J. E. P. Dahl, R. M. K. Carlson, H. Shinohara, D. Tomanek, *ACS Nano* **2012**, *6*, 8674 – 8683.
[133] D. A. Britz, A. N. Khlobystov, K. Porfyrakis, A. Ardavan, G. A. D. Briggs, *Chem. Commun.* **2005**, 37 – 39.
[134] J. Zhang, Y. Miyata, R. Kitaura, H. Shinohara, *Nanoscale* **2011**, *3*, 4190 – 4194.
[135] J. Zhang, Z. Zhu, Y. Q. Feng, H. Ishiwata, Y. Miyata, R. Kitaura, J. E. P. Dahl, R. M. K. Carlson, N. A. Fokina, P. R. Schreiner, *Angew. Chem.* **2013**, *125*, 3805 – 3809; *Angew. Chem. Int. Ed.* **2013**, *52*, 3717 – 3721.
[136] G. C. McIntosh, M. Yoon, S. Berber, D. Tomanek, *Phys. Rev. B* **2004**, *70*, 045401.
[137] W. Piekarczyk, *J. Mater. Sci.* **1998**, *33*, 3443 – 3453.
[138] D. Stojkovic, P. Zhang, V. H. Crespi, *Phys. Rev. Lett.* **2001**, *87*, 125502.
[139] L.-M. Peng, Z. L. Zhang, Z. Q. Xue, Q. D. Wu, Z. N. Gu, D. G. Pettifor, *Phys. Rev. Lett.* **2000**, *85*, 3249.
[140] O. A. Shenderova, V. V. Zhirnov, D. W. Brenner, *Crit. Rev. Solid State Mater. Sci.* **2002**, *27*, 227 – 356.
[141] J. T. Tanskanen, M. Linnolahti, A. J. Karttunen, T. A. Pakkanen, *J. Phys. Chem. C* **2008**, *112*, 11122 – 11129.
[142] F. L. Liu, *Phys. Chem. Chem. Phys.* **2004**, *6*, 906 – 909.
[143] F. L. Liu, L. Peng, J. X. Zhao, S. Q. Wang, *Int. J. Quantum Chem.* **2005**, *103*, 167 – 175.
[144] J. N. Coleman, U. Khan, W. J. Blau, Y. K. Gun′ko, *Carbon* **2006**, *44*, 1624 – 1652.
[145] J. Guo, B. Wen, R. Melnik, S. Yao, T. Li, *Diamond Relat. Mater.* **2011**, *20*, 551 – 555.
[146] F. Occelli, P. Loubeyre, R. Letoullec, *Nat. Mater.* **2003**, *2*, 151 – 154.

[147] T. Yamanaka, S. Morimoto, H. Kanda, *Phys. Rev. B* **1994**, *49*, 9341 – 9343.
[148] H. Cynn, J. E. Klepeis, C. S. Yoo, D. A. Young, *Phys. Rev. Lett.* **2002**, *88*, 135701.
[149] H. Peelaers, B. Partoens, F. M. Peeters, *Nano Lett.* **2009**, *9*, 107 – 111.
[150] H. Peelaers, B. Partoens, F. M. Peeters, *Appl. Phys. Lett.* **2009**, *95*, 122110.
[151] A. Trejo, A. Miranda, L. Rivera, A. Diaz-mendez, M. Cruz-Irisson, *Microelectron. Eng.* **2012**, *90*, 92 – 95.
[152] K. W. Sun, J. Y. Wang, T. Y. Ko, *Appl. Phys. Lett.* **2008**, *92*, 153115.
[153] C. W. Padgett, D. W. Brenner, *Nano Lett.* **2004**, *4*, 1051 – 1053.
[154] N. V. Novikov, A. P. Podoba, S. V. Shmegera, A. Witek, A. M. Zaitsev, A. B. Denisenko, W. R. Fahmer, M. Werner, *Diamond Relat. Mater.* **1999**, *8*, 1602 – 1606.
[155] J. F. Moreland, J. B. Freund, G. Chen, *Microscale Thermophys. Eng.* **2004**, *8*, 61 – 69.
[156] C. W. Padgett, O. Shenderova, D. W. Brenner, *Nano Lett.* **2006**, *6*, 1827 – 1831.
[157] J. Guo, B. Wen, R. Melnik, S. Yao, T. Li, *Phys. E* **2010**, *43*, 155 – 160.
[158] R. L. McCreery, *Chem. Rev.* **2008**, *108*, 2646 – 2687.
[159] P. Subramanian, Y. Coffinier, D. Steinmuller-Nethl, J. Foord, R. Boukherroub, S. Szunerits, *Electrochim. Acta* **2013**, *110*, 4 – 8.
[160] A. Socoliuc, *Science* **2006**, *313*, 207 – 210.
[161] W. Wu, L. Bai, X. Liu, Z. Tang, Z. Gu, *Electrochem. Commun.* **2011**, *13*, 872 – 874.
[162] M. Lv, M. Wei, F. Rong, C. Terashima, A. Fujishima, Z. Gu, *Electroanalysis* **2010**, *22*, 199 – 203.
[163] Y. Yang, J. Oh, Y. Kim, C. Terashima, A. Fujishima, J. Kim, H. Kim, *Chem. Commun.* **2010**, *46*, 5793 – 5795.
[164] N. Yang, R. Hoffmann, W. Smirnov, A. Kriele, C. E. Nebel, *Electrochem. Commun.* **2010**, *12*, 1218 – 1221.
[165] F. J. Himpsel, J. A. Knapp, J. A. Vanvechten, D. E. Eastman, *Phys. Rev. B* **1979**, *20*, 624 – 627.
[166] B. J. Cui, J. Ristein, L. Ley, *Phys. Rev. Lett.* **1998**, *81*, 429 – 432.
[167] T. Ito, M. Nishimura, M. Yokoyama, M. Irie, C. L. Wang, *Diamond Relat. Mater.* **2000**, *9*, 1561 – 1568.
[168] I. L. Krainsky,, V. M. Asnin, G. T. Mearini, J. A. Dayton, *Phys. Rev. B* **1996**, *53*, R7650 – R7653.
[169] Y. K. Chang, H. H. Hsieh, W. F. Pong, M. H. Tsai, F. Z. Chien, P. K. Tseng, L. C. Chen, T. Y. Wang, K. H. Chen, D. M. Bhusari, J. R. Yang, S. T. Lin, *Phys. Rev. Lett.* **1999**, *82*, 5377 – 5380.
[170] C. Wang, A. Garcia, D. C. Ingram, M. Lake, M. E. Kordesch, *Electron. Lett.* **1991**, *27*, 1459 – 1461.
[171] Y. F. Tzeng, K. H. Liu, Y. C. Lee, S. J. Lin, I. N. Lin, C. Y. Lee, H. T. Chiu, *Nanotechnology* **2007**, *18*, 435703.
[172] Y. S. Zou, K. L. Ma, W. J. Zhang, Q. Ye, Z. Q. Yao, Y. M. Chong, S. T. Lee, *Diamond Relat. Mater.* **2007**, *16*, 1208 – 1212.
[173] N. Jiang, K. Eguchi, S. Noguchi, T. Inaoka, Y. Shintani, *J. Cryst. Growth* **2002**, *236*, 577 – 582.
[174] S. Gupta, B. L. Weiss, B. R. Weiner, G. Morel, *Appl. Phys. Lett.* **2001**, *79*, 3446 – 3448.
[175] L. Gan, E. Baskin, C. Saguy, R. Kalish, *Phys. Rev. Lett.* **2006**, *96*, 196808.
[176] K. J. Sankaran, Y. F. Lin, W. B. Jian, H. C. Chen, K. Panda, B. Sundaravel, C. L. Dong, N. H. Tai, I. N. Lin, *ACS Appl. Mater. Interfaces* **2013**, *5*, 1294 – 1301.
[177] W. Zhu, G. P. Kochanski, S. Jin, *Science* **1998**, *282*, 1471 – 1473.
[178] D. Pradhan, I. N. Lin, *ACS Appl. Mater. Interfaces* **2009**, *1*, 1444 – 1450.
[179] J. P. Thomas, H. C. Chen, N. H. Tai, I. N. Lin, *ACS Appl. Mater. Interfaces* **2011**, *3*, 4007 – 4013.
[180] Q. H. Wang, A. A. Setlur, J. M. Lauerhaas, J. Y. Dai, E. W. Seeling, R. P. H. Chang, *Appl. Phys. Lett.* **1998**, *72*, 2912 – 2913.
[181] M. Najam-ul-Haq, M. Rainer, C. W. Huck, P. Hausberger, H. Kraushaar, G. K. Bonn, *Anal. Chem.* **2008**, *80*, 7467 – 7472.
[182] J. M. Kim, J. H. Park, C. W. Baek, Y. K. Kim, *J. Microelectromech. Syst.* **2004**, *13*, 1036 – 1042.
[183] M. Adamschik, J. Kuserer, P. Schmid, K. B. Schad, D. Grobe, E. Kohn, *Diamond Relat. Mater.* **2002**, *11*, 672 – 676.
[184] V. P. Adiga, A. V. Sumant, S. Suresh, C. Gudeman, O. Auiello, J. A. Carlisle, R. W. Carpick, *Phys. Rev. B* **2009**, *79*, 245403.
[185] S. Koizumi, K. Watanabe, M. Hasegawa, H. Kanda, *Science* **2001**, *292*, 1899 – 1901.
[186] H. El-Hajj, A. Denisenko, A. Kaiser, R. S. Balmer, E. Kohn, *Diamond Relat. Mater.* **2008**, *17*, 1259 – 1263.
[187] R. A. Oliver, *Rep. Prog. Phys.* **2008**, *71*, 076501.
[188] P. Niedermann, W. Hänni, N. Blanc, R. Christoph, J. Burger, *J. Vac. Sci. Technol. A* **1996**, *14*, 1233 – 1236.
[189] W. Kulisch, A. Malave, W. Scholz, C. Mihalcea, E. Oesterschulze, G. Lippold, *Diamond Relat. Mater.* **1997**, *6*, 906 – 911.
[190] T. Hantschel, P. Niedermann, T. Trenkler, W. Vandervorst, *Appl. Phys. Lett.* **2000**, *76*, 1603 – 1605.
[191] H. J. Dai, J. H. Hafner, A. G. Rinzler, D. T. Colbert, R. E. Smalley, *Nature* **1996**, *384*, 147 – 150.
[192] G. Jänchen, P. Hoffmann, A. Kriele, H. Lorenz, A. J. Kulik, G. Dietler, *Appl. Phys. Lett.* **2002**, *80*, 4623 – 4625.
[193] M. J. Burek, N. P. de Leon, B. J. Shields, B. J. M. Hausmann, Y. W. Chu, Q. M. Quan, A. S. Zibrov, H. Park, M. D. Lukin, M. Loncar, *Nano Lett.* **2012**, *12*, 6084 – 6089.
[194] M. J. Burek, D. Ramos, P. Patel, I. W. Frank, M. Loncar, *Appl. Phys. Lett.* **2013**, *103*, 131904.
[195] B. J. M. Hausmann, B. J. Shields, Q. M. Quan, Y. Chu, N. P. de Leon, R. Evans, M. J. Burek, A. S. Zibrov, M. Markham, D. J. Twitchen, *Nano Lett.* **2013**, *13*, 5791 – 5796.
[196] G. Carpini, F. Lucarelli, G. Marrazza, M. Mascini, *Biosens. Bioelectron.* **2004**, *20*, 167 – 175.
[197] O. Pänke, A. Kirbs, F. Lisdat, *Biosens. Bioelectron.* **2007**, *22*, 2656 – 2662.
[198] H. Aoki, H. Tao, *Analyst* **2005**, *130*, 1478 – 1482.
[199] G. Zhao, Y. Qi, Y. Tian, *Electroanalysis* **2006**, *18*, 830 – 834.
[200] W. Huang, G. Mai, Y. Liu, C. Yang, W. Qua, *J. Nanosci. Nanotechnol.* **2004**, *4*, 423 – 427.
[201] Q. Wang, A. Vasilescu, P. Subramanian, A. Veronica, V. Andrei, Y. Coffinier, M. Li, R. Boukherroub, S. Szunerits, *Electrochem. Commun.* **2013**, *35*, 84 – 87.